

Cold Cathode Materials for Pseudospark Switches

by

Shaomao Li

A thesis submitted to the Graduate Faculty of
Auburn University
in partial fulfillment of the
requirements for the Degree of
Master of Science

Auburn, Alabama
May 14, 2010

Keywords: pseudospark switch, carbon nanotubes, pulse power,
trigger, field emission, breakdown

Copyright 2009 by Shaomao Li

Approved by

Hulya Kirkici, Chair, Associate Professor of Electrical and Computer Engineering
Mark Nelms, Professor of Electrical and Computer Engineering
Michael Baginski, Associate Professor of Electrical and Computer Engineering

Abstract

In general, for plasma switches, the initiation of the plasma is critical and this is usually achieved by a “trigger” scheme. The seed electrons needed to initiate a breakdown can be generated by several means such as thermionic, field or optical emission. While the thermionic emission has been used mainly in vacuum tubes and is a mature technology, field emission (or cold-cathode electron emission) has been the subject of recent studies and technology. The efficiency of these seed electron emission determines how well the plasma switch can close or open. It is known that the carbon nano tubes (CNTs) have excellent field emission characteristic under high vacuum pressure of 10^{-7} to 10^{-6} Torr and they have been considered as prima candidates as cold-cathode electron emitters. On the other hand, most plasma switches operate at mTorr pressure ranges, which is relatively higher than the vacuum pressure levels mentioned above. Therefore, the electron emission characteristics of CNTs in elevated pressures higher than vacuum need to be known to evaluate possible use of them as trigger electrode. The purpose of this research is to observe the field emission characteristics of several different kinds of CNT samples and other nano materials in background pressures ranging from 10^{-3} Torr to 1 Torr.

Acknowledgments

First of all, I would like to thank my advisor, Dr. Kirkici, for offering me the opportunity to explore the wonderful research world. Her constant guidance and encouragement is indispensable for me to carry out this work.

Secondly, I want to thank Dr.Koppisetty and Dr.Chen, who graduated from Auburn University. The knowledge and the way of conducting scientific research I learned from them are invaluable and priceless.

Thirdly, I thank my mother Xiaofen Chen, and my father Qifu Li, for their love, encouragement and supports.

Finally, but not the least importantly, I want to thank my colleagues and collaborators: Mark L.Lipham, Haitao Zhao, Esin Sozer, Ramesh Bokka. I also thank the Technical Support: Linda Barresi and Calvin Cutshaw and the other people who gave their precious help. Without their efforts, this work would be impossible

Table of Contents

Abstract	ii
Acknowledgments	iii
List of Tables	vi
List of Figures	vii
Chapter 1 Introduction	1
Chapter 2 Background.....	3
2.1 Pulsed Power Engineering.....	3
2.2 Switches	6
2.2.1 Closing Switches.....	8
2.2.2 Opening Switches.....	13
2.3 Pseudospark Switches	15
2.3.1 Hollow Cathode Discharge	15
2.3.2 Pseudospark Discharge.....	16
2.4 Triggering Mechanisms.....	18
2.4.1 Pulsed Low-Current Glow Discharge:	19
2.4.2 Surface Discharge Triggering:	19
2.4.3 Optical Triggering	20
2.5 Field Emission Materials Literature Review.....	22
Chapter 3 Carbon Nanotubes.....	25
3.1 Carbon Nanotubes and Structure.....	25
3.2 Properties of Carbon Nanotubes	29

3.3 Synthesis of CNTs	30
3.3.1 Growth Mechanism	30
3.3.2 Arc Discharge Method	31
3.3.3 Laser Ablation Method	33
3.3.4 Chemical Vapor Deposition	34
Chapter 4 Field Emission Experiment	37
4.1 Research Objective.....	37
4.2 Experiment Setup.....	38
4.3 Field Emission Characteristics of CNTs.....	40
4.3.1 SEM Images of CNTs.....	40
4.3.2 Field Emission Intensity	43
4.4 Field Emission of Zinc Oxide (ZnO)	48
4.5 Field Emission of Oxygen-free Copper	50
4.6 Field Emission of Nanocrystalline Diamond.....	53
Chapter 5 Summary	56
References	59

List of Tables

Table 2.1 Summary of properties of closing switch.....	14
Table 4.1 SEM image of CNT before experiment	41
Table 4.2 SEM image of CNT after experiment	42
Table 5.1 Comparison of different materials field emission	57

List of Figures

Figure 2.1 Pulse Shape.....	4
Figure 2.2 General scheme of a pulse power generator	5
Figure 2.3 Generator with capacitive energy storage and closing switch.....	5
Figure 2.4 Generator with inductive energy storage and opening switch	6
Figure 2.5 Components of a typical closing switch.....	9
Figure 2.6 Rang of gas pressures and operating voltage for gas switches	10
Figure 2.7 Evolution of voltage, current and power loss in gas switches	10
Figure 2.8 Structure of thyristor and two transistors equivalent circuit.....	11
Figure 2.9 A four-stage repetitive thyristor switch	12
Figure 2.10 Basic circuit with capacitive energy and a ferromagnetic switch	13
Figure 2.11 Electric field configuration of typical pseudospark geometry	16
Figure 2.12 Cross sectional view of an electrical triggered pseudospark switch	17
Figure 2.13 Schematic drawing of pseudospark switch with pulsed glow discharge trigger.....	19
Figure 2.14 Schematic drawing of pseudospark switch triggered by surface discharge.....	20
Figure 3.1 Buckyball structure.....	26
Figure 3.2 Classification of CNTs: (a) armchair, (b) zigzag, and (c) chiral nanotubes	27
Figure 3.3 Structures of MWCNTs	28
Figure 3.4 Schematics of the growth mechanism: (a) root growth and (b) tip growth	31
Figure 3.5 Schematic diagram of the arc apparatus	32

Figure 3.6 Schematics of experimental setup of laser ablation technique	33
Figure 3.7 Schematic diagram of a PECVD setup for carbon nanotubes growth	35
Figure 4.1 Circuit diagram of field emission intensity measurement set-up.....	39
Figure 4. 2 SEM image of Aligned MWCNT with a tilted angle of 20 degrees, 500 resolution. .	41
Figure 4.3 SEM image of Aligned MWCNT, top view with resolution of 10,000.....	41
Figure 4.4 SEM image of Random MWCNT, top view with resolution of 10,000.....	41
Figure 4.5 SEM image of Random SWCNT, top view with resolution of 20,000.....	41
Figure4.6 SEM image of the entire filed emission area of Random MWCNT , top view with resolution of 20	42
FIGURE 4.7 SEM image of the comparison between filed emission area (lower white part) and non filed emission area (upper dark part),Random MWCNT, top view with resolution of 950	42
Figure 4.8 SEM image of Random SWCNT, top view with resolution of 20,000	42
Figure 4.9 Field emission characteristics of three samples used in the experiments	44
Figure 4.10 Field emission of Random MWCNT in different pressures of air	45
Figure 4.11 Field emission of Aligned MWCNT in different pressures of He.....	45
Figure 4.12 Field emission of Random SWCNT in different pressures of air	46
Figure 4.13 Comparison of samples' field emission in air and He	47
Figure 4.14 SEM images of ZnO sample surface with 15,000 resolution	48
Figure4.15 Field emission characteristic of ZnO nanorods at pressure of 10^{-6} Torr	49
Figure 4.16 Field emission characteristic of ZnO nanorods at pressure of 2×10^{-2} Torr.....	50
Figure 4.17 SEM images of Oxygen-free copper surface with 15,000 resolution	51
Figure 4.18 Field emission characteristic of Oxygen-free copper at pressure of 4×10^{-6} Torr.....	51

Figure 4.19 Field emission characteristic of Oxygen-free copper at pressure of 1×10^{-5} Torr.....	52
Figure 4.20 Field emission characteristic of Oxygen-free copper at pressure of 2×10^{-2} Torr.....	52
Figure 4.21 SEM images of nanocrystalline diamond surface with 10,000 resolution	53
Figure 4.22 SEM images of nanocrystalline diamond surface with 100,000 resolution.....	54
Figure 4.23 Field emission characteristic of nanocrystalline diamond at pressure of 10^{-1} Torr	55
Figure 4.24 Field emission characteristic of nanocrystalline diamond at pressure of 5×10^{-1} Torr.....	55

CHAPTER 1

INTRODUCTION

Pseudospark switches are characterized by high current emission and conduction while operating in glow discharge mode due to the hollow-cathode and hollow-anode geometry used in the construction. The operating cycles of these switches are the hold-off voltage, triggering, conduction phase, and recovery phase. Triggering greatly affects the operating characteristics such as delay, jitter, and repetition of these switches. Due to the demand for the high current (or high current density), a hollow cathode structure is the most suitable geometry, because orders of magnitude larger current densities can be achieved relative to the planar electrode structure [1]. In general, there are three main methods to trigger pseudospark switches, namely surface discharge triggering [2], optical triggering [3], and pulsed low-current glow discharge triggering. In this paper, we investigate the possibility of using CNTs as the cold electron emitter to be used as the trigger electrode for a pseudospark switch.

CNTs, discovered by Iijima in 1991[4], have been attracting extensive attention in research. Rinzler et al made the first report on the field emission from CNTs in 1995 [5]. As a result of significant improvement in recent processing techniques, the CNTs demonstrate better qualities as the promising cold cathode material in field emission devices. Their remarkable field emission properties are attributed to their high chemical stability, high mechanical strength, high aspect ratio and high current carrying capacity.

Furthermore, most reported field emission characteristics of CNTs have been measured

at high vacuum pressure of around 1×10^{-6} and 1×10^{-7} Torr (1 Torr=133.322 Pa). On the other hand, the typical operating pressures of pseudospark switches are in the range of 0.001 to 1.0 Torr. Therefore, if these materials are to be used as a trigger for these types of plasma switches, then their electron emission characteristics have to be measured in these pressure ranges. This work reports the field emission characteristics of CNTs at varying pressures from 1×10^{-6} up to 1 Torr.

Besides CNTs, this work also presents the field emission characteristics of other materials, such as copper, nanocrystalline diamond and nanorod ZnO. Some of them are proved to be good candidate as trigger electrode materials for pseudospark switches.

CHAPTER 2

BACKGROUND

2.1 Pulsed Power Engineering

Pulse power engineering is the science and technology of storing energy over a relatively long period of time and releasing it in a relatively short time thus increasing the instantaneous power. Pulse electric field is considered “pulsed power” if instantaneous electrical power of the pulse is around 10^9 W, and its energy content is of the order of 10^3 J or greater. So far, the highest energy and power that have been achieved in a single pulse are in order of 100 MJ and 100 terawatts respectively [6]. The corresponding voltage is from 10^4 - 5×10^7 V, and the corresponding current is between 10^3 and 10^7 A.

In addition to its power and energy, pulse electric field has another important characteristic that is the shape of pulse, defined by its rise and fall times, duration, and flatness of its plateau region. Usually, the duration of a power pulse lies between 10^{-9} – 10^{-6} seconds, depending on the application. The typical pulse shape is shown in Figure 2.1.

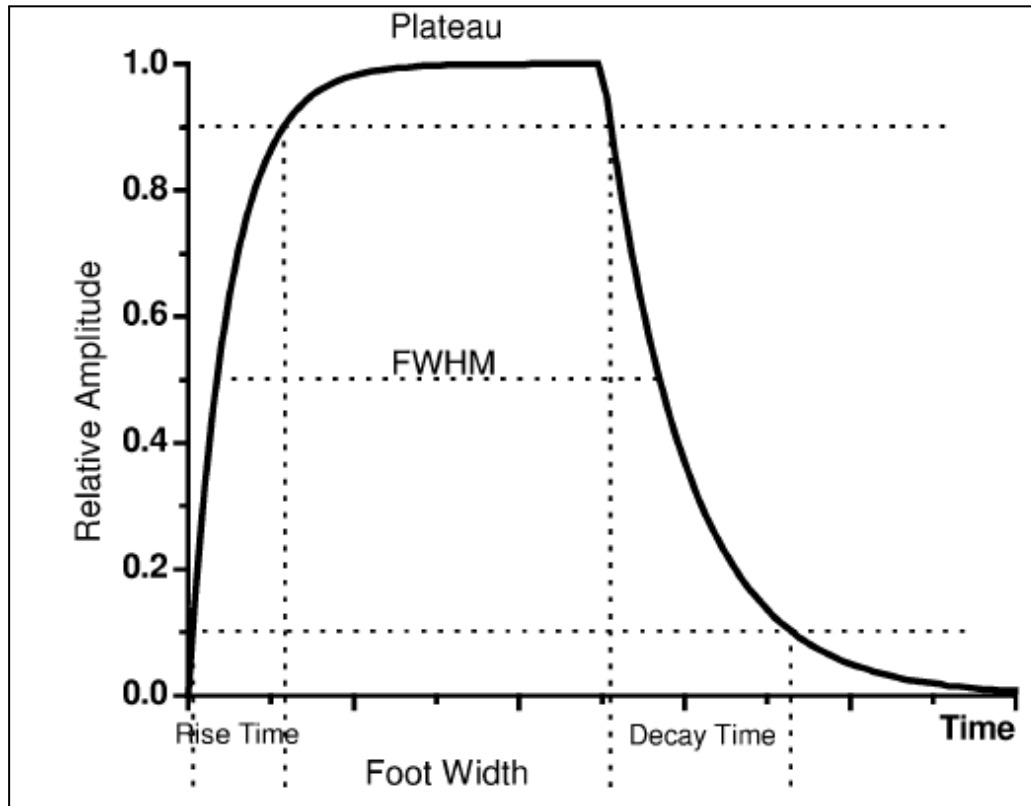


Figure 2.1 Pulse Shape

Rise Time: The time it takes for the voltage to rise from 10% to 90% of its peak voltage

Decay Time: The time it takes for the voltage to decrease from 90% to 10% of its peak voltage, it is also called fall time.

Pulse Duration: There is no unique definition, sometimes it means the full time width between rise and decay half maximum of the pulse (FWHM). However, for some applications, it is defined as the time it remains at 90% of its maximum value.

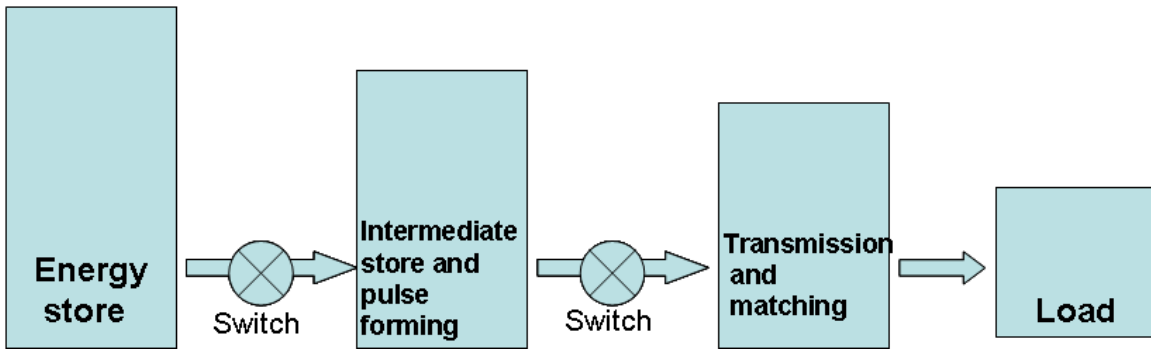


Figure 2.2 General scheme of a pulse power generator

The components of a pulse power generator are sketched schematically in Figure 2.2. Energy can be stored in several forms: chemical, mechanical and electrical. By using appropriate switches, the desired shape, rise and decay time of the pulse could be achieved. An impedance matching network may also become necessary for optimal energy transfer to the load.

Electrical energy can be stored either capacitively in an electric field or inductively in a magnetic field.

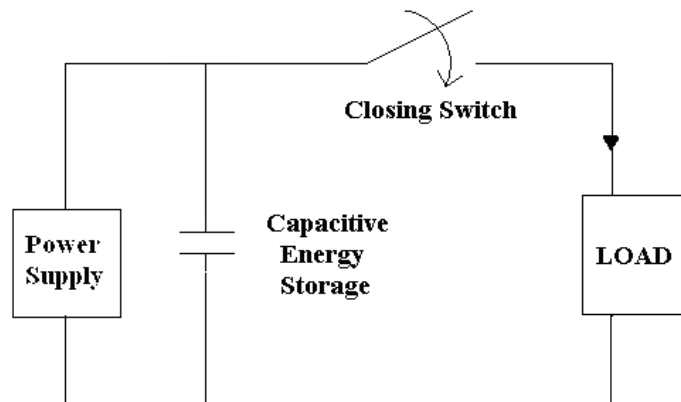


Figure 2.3 Generator with capacitive energy storage and closing switch

Figure 2.3 shows the capacitive energy storage schematically. Capacitive pulse power generators are designed mostly with closing switches which are shown in Figure 2.3. The capacitor is charged by the power supply, and holds the charging voltage while closing switch

remains open. Once the switch closes, the energy in the capacitor is transferred to the load immediately. Therefore, through the whole process, the generator will achieve output power multiplication by current amplification.

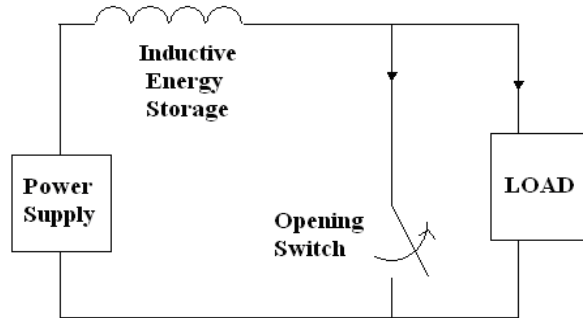


Figure 2.4 Generator with inductive energy storage and opening switch

A typical inductive pulse power generator indicated in Figure 2.4 consists of inductive energy storage, opening switches, power supply and load. Energy from power supply is delivered and saved in inductive energy storage during the time opening switch keeps close. And there is a large current is stored in the inductor during this stage. After completion of charging process, the switch will open. Because of applying voltage amplification, the generator achieves power multiplication.

Since it is harder to build suitable opening switches, most pulsed power generators use capacitive energy storage despite the fact that the energy density in capacitive storage is much smaller than that in inductive storage.

2.2 Switches

In pulsed power applications, switches need to be capable of handling power level of about tera-watt (10^{12} W) and having jitter time in the order of nanosecond (10^{-9} s). The conventional switches, such as high voltage switch gears, are no longer adequate to meet these

requirements. It is necessary to develop new types of switches, which can handle such high level of power (10^{12} W) and have such low jitter time (10^{-9} s). On the basis of the technique employed for transferring the energy, high energy power switches may be classified into two types: closing and opening switches. High energy storage system requires different types of switches. Capacitive energy storage requires closing switches and inductive energy storage needs opening switches.

The basic principle of switching is relatively simple: at the proper time, the property of the switch medium changes from insulating status to conducting status or the Vis-verse. Although the principle is simple, in reality it is complex and difficult to achieve accuracy and effectiveness with switches. It involves not only the parameters of switches but also many physical and chemical processes during the change of the switch stage, some of which are still unexplainable.

The common parameters of switches are listed below:

Trigger Pulse: A fast pulse supplied externally to initiate the action of switching

Hold-Off Voltage: The maximum static voltage that can be applied to the switch before breakdown between the main electrodes occurs.

Voltage Fall Time: After breakdown is initiated, the time interval during which the voltage drops from the value of hold-off to that of the conduction voltage.

Conduction Drop: The voltage drop across the switch impedance during conduction.

Jitter: Statistical variations in the exact time of the initiation of conduction with respect to the trigger signal.

Recover Time: The time interval during which the voltage reverses its polarity.

Repetition Rate: The rate at which the switch can be closed and opened without degradation of

characteristics.

Delay Time: The time interval between the time the trigger pulse is at its peak value and the point at which switch starts to close or open.

Current Rise Time: The time interval required for the current to rise from 10% to 90% of its peak value.

Recharge Time: The time interval between the end of the recover time and the point at which the voltage recovers to the hold-off value.

Current Pulse Width: The time duration corresponds to the full width at half maximum of the current pulse.

Peak Power: The maximum value of the product of voltage and current which occur at the same time.

Transfer Energy: the Time integral of the product of voltage and current.

Life Time: Under normal operating conditions, the total number of switching operations beyond which the switch can no longer function properly.

Reliability: A measure of the ratio between the numbers of successful operations to the total number of operations within the life time of the switch.

2.2.1 Closing Switches

Closing switches are “open” naturally and are “closed” with an application of some sort of external trigger or as a result of its own overvoltage. Basically, closing switches have various types such as gas-filled switches, semiconductor closing switches and magnetic switches.

Table 2.1 summarizes the operating characteristics of some of these switches.

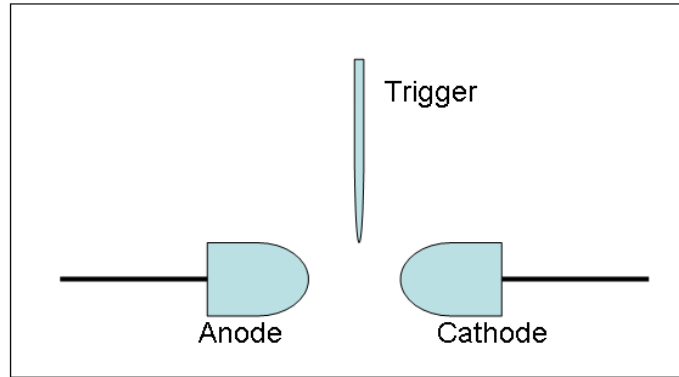


Figure 2.5 Schematics of a typical closing switch

2.2.1.1 Gas-Filled Switches

Figure 2.5 shows basic geometry of a gas-filled switch. Gas-Filled switches are easy to use, able to handle large currents and charges and can be triggered easily. Different types of gas switches operate in their specific pressure ranges. Figure 2.6 shows the range of operating pressure and voltage for some of the most common types of gas-filled switches. These include thyratrons, pseudospark switches, ignitrons, krytrons, and spark gaps. In addition, Paschen curve for air with the fixed gap width of 3 mm is overlaid as reference to the breakdown voltage of gaseous media. As seen in Figure 2.6, all the gas-filled switches operate below the Paschen curve. Above this curve, the normal operating voltage will exceed the breakdown strength of the gaseous, and will cause unexpected breakdown events.

Nearly all types of gas-filled switches are operated on the basic principle of ionization and breakdown of gases. Under normal conditions (below its breakdown voltage), gas is an insulator and becomes conducting when ionized.

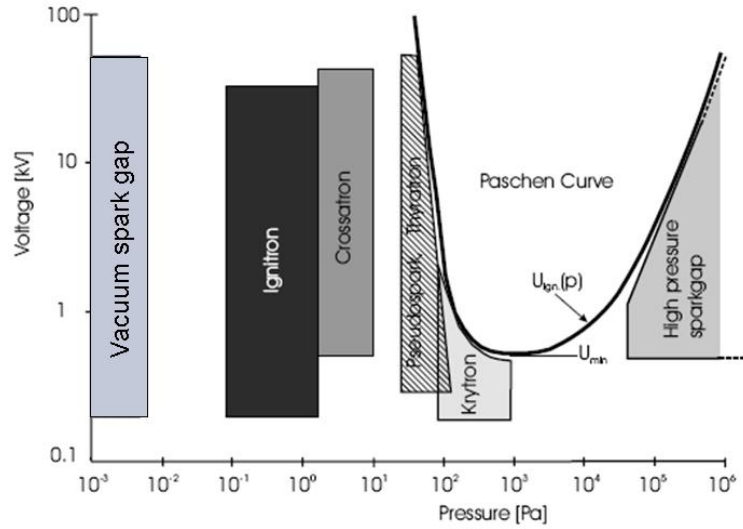


Figure 2.6 Rang of gas pressures and operating voltage for gas switches [6]

The operation of the gas-filled switches can be divided into four phases schematically shown in Figure 2.7:

- I. Trigger phase (built up a trigger discharge).
- II. Transition phase (transition from high to low switch impedance).
- III. Stationary phase (constant conductivity of the switch).
- IV. Recovery phase (restoration of the previous electric strength).

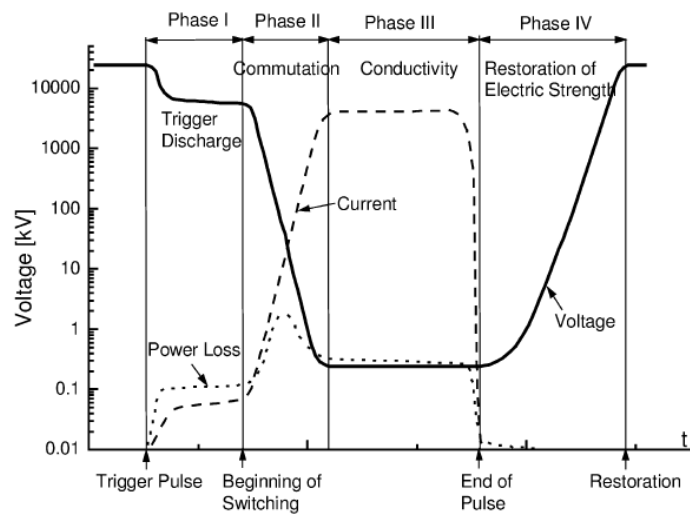


Figure 2.7 Evolution of voltage, current and power loss in gas switches

2.2.1.2 Semiconductor Closing Switches

The relatively low mobility and density of charge carrier in the “plasma” are the two of the limiting characteristics of semiconductor closing switches. Therefore, in order to conduct large currents, a large volume of the conducting region is needed, which means increasing the area of current-carrying channel.

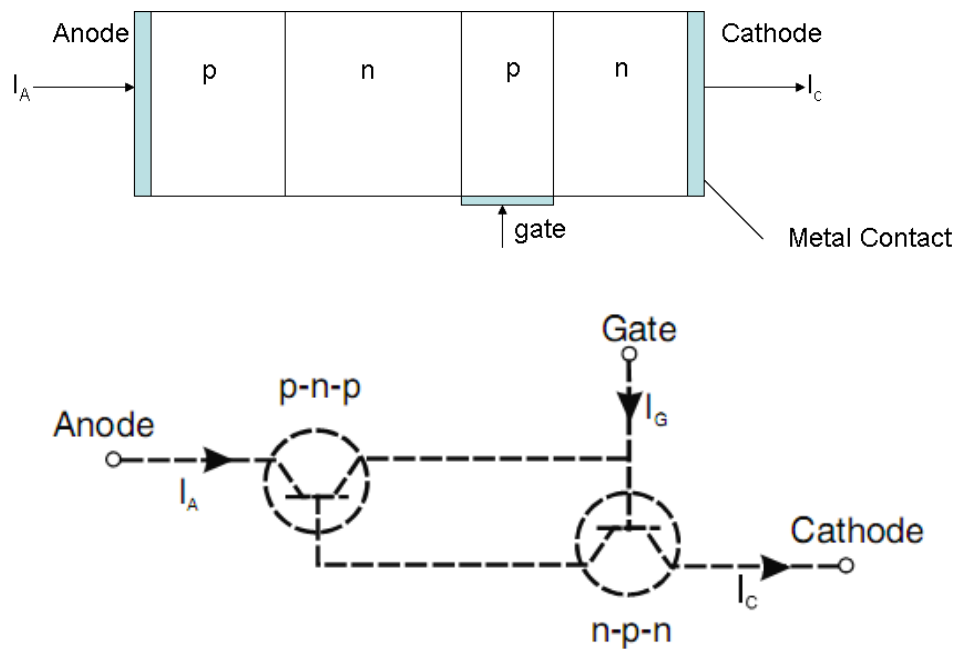


Figure 2.8 Structure of thyristor and two transistors equivalent circuit

Thyristors and insulated-gate bipolar transistor (IGBTs) are the main two types of semiconductor closing switches. Thyristor is a four-layer device with the sequence $p^+n^-pn^+$, which can be considered as a combination of a p-n-p and an n-p-n transistor sharing a common collector junction shown in Figure 2.8.



Figure 2.9 A four-stage repetitive thyristor switch

In Table 2.1, we can find that, for a common thyristor, the hold-off voltage is less than 5 kV, and the peak current is less than 5 kA. Figure 2.9 shows a four-stage thyristor switch, whose hold-off voltage can be up to 10 kV and the peak current can be up to 30 kA. The maximum current rise is $20 \text{ kA}/\mu\text{s}$ and the repetition rate can be from 10- 50 Hz.

IGBT is another important semiconductor, which combines the advantages of bipolar transistors (low resistance in switch-on state) with those of field effect transistors (low free gate control). Single IGBT unite has a lower current capability than thyristors in the range of 1000-1800 V. However, it is easy to arrange them in parallel, with switch-on rise times of the order of several 10ns. High-power IGBTs are being used in industry with blocking voltages up to 4 kV and on-state currents of 3 kA.

Although semiconductors are widely used in high voltage power suppliers and charging units, it is still unrealistic to use them as high voltage switches in pulsed power area because of high complexity and high cost.

2.2.1.3 Magnetic Switches

Magnetic switches operate based on the saturation of a ferromagnetic core. The good aspects of them are that they can operate with relatively small losses and without wear. Figure 2.10 shows the basic circuit used with a magnetic switch.

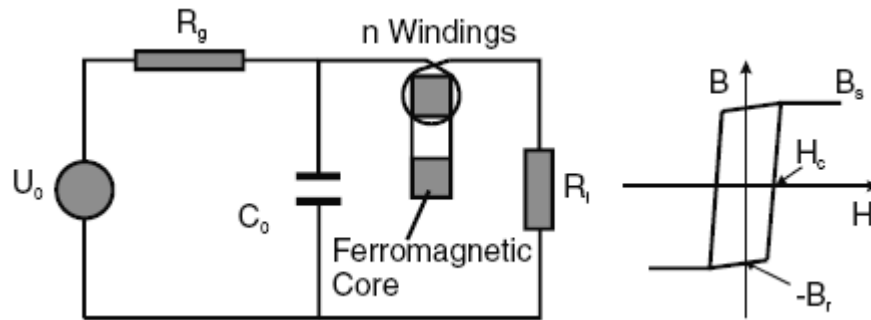


Figure 2.10 Basic circuit with capacitive energy and a ferromagnetic switch

There is a high inductance of the coil at the beginning while the capacitor is being charged. When saturation of the core is reached by the leakage current flowing through the coil, the inductance drops abruptly and the switch is closed.

2.2.2 Opening Switches

An opening switch is characterized by a sudden increase in impedance. This can be initiated either by an external actuator or by some internal processes. The mechanism of opening can be of resistive, inductive and capacitive nature. Fuse is a typical resistive opening switch. Inductive opening switches can be realized by flux compression, such that $L(t) > L(0)$. A capacitive opening can be obtained if $C(t) < C(0)$.

Opening switches also have several types, such as superconducting opening switch, plasma opening switch, plasma flow switch and others. They will not be discussed in this work, however, further details of opening switches can be found in [6].

Table 2.1 Summary of properties of closing switch [6]

Type	Hold-off potential (kV)	Peak current (kA)	Cumulative Charge (As)	Repetition rate (Hz)	Life time	Remarks
Spark gap	1-6000	10^{-3} -1000	0.1-50	1-10	10^3 - 10^7	Life time is determined by electrode erosion
Thyratron	5-50	0.1-10	10^{-3}	1000	10^7 - 10^8	Applied in lasers and accelerators
Ignitron	>10	>100	2000	1	10^5 - 10^6	Applied in lasers and accelerators
Pseudospark switch	1-50	1-20	1	1-1000	10^6 - 10^8	Similar to thyratron
Krytron	8	3	0.01-0.1	<1000	10^7	Short delay
Magnetic switch	1000	100-1000		10	10^8 - 10^9	Cannot be triggered; one operating point only
Thyristor	<5	<5	10^{-2}	10	10^8	Can be stacked, expensive, complex
IGBT	<4	3		100	10^8	Can be switched off

2.3 Pseudospark Switches

Pseudospark switches have several advantages over some existing switch technologies in the pulsed power regime, and combine the advantages of pressurized spark gaps and thyratron. Particularly, pulse repetition of pseudospark switches can be up to several kHz at peak currents of tens of kA, while having the ability of full current reversal. They have a small anode delay time jitter of a few ns only, and are scalable to peak currents of over 100 kA, with which current rise rate is of over 5×10^{11} A/s. Furthermore lifetimes of several hundred kC, which is 5-10 times that of state-of-the-art spark gaps can be achieved.

2.3.1 Hollow Cathode Discharge

Pseudospark switch, like a conditional thyratron, operates in a low pressure regime, and operates based on the principles of a hollow cathode discharge. The hollow cathode effect is mainly caused by pendulum electrons, special electrons found in hollow cathode discharge. Electrons emitted from the cathode surface reflect back and forth between the cathode sheaths, which undergo many ionizing collisions, leading to high electron emission rates. Cathode fall can be significantly thinner in hollow cathode geometries leading to increased ion velocities and increased secondary electron emission rates. Thus, hollow structure increases the probability of multiple processes and collisions for all particles creating high current density plasma inside the hollow cathode [7].

In general, operating region of the hollow cathode discharge range in literature for rare gases is $1 \text{ torr-cm} < pd < 10 \text{ torr-cm}$ where p is pressure and d is the diameter of hollow cavity [7].

2.3.2 Pseudospark Discharge

Pseudospark is a gas discharge, which occurs in a special geometry of the discharge chamber at typical pressures of 1 mTorr – 1 Torr. As we can see in Figure 2.11, the chamber consists of two electrodes with a distance of typically 3-5 mm and a centric borehole of 3-5 mm in diameter. The discharge starts in the hollow cathode behind the borehole. Fast current rise of the hollow cathode discharge and the transition to a vacuum arc-like discharge at higher current (>1 kA) makes the pseudospark an interesting phenomenon for pulsed power technology.

Figure 2.11 shows electric field lines at the axis of hollow cathode and hollow anode geometry causing breakdown voltage drop in this region.

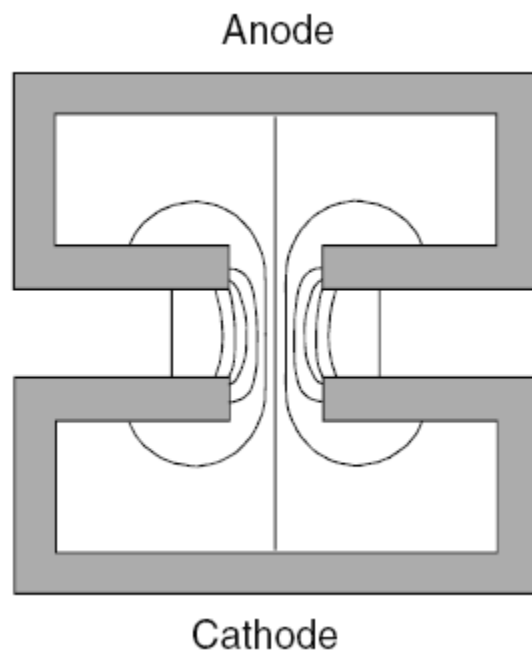


Figure 2.11 Electric field configuration of typical pseudospark geometry

With the help of a small number of seed electrons, which can be created, for example, by a trigger glow discharge, a pseudospark discharge can be initiated. Initially, most electrons are runaway electrons, i.e., they become accelerated to energies comparable to the potential drop between the anode and cathode.

The switching mechanism is based on the build-up of highly ionized plasma. Plasma first occurs inside the hollow cathode due to the low E/P (low pressure). Then there is ionization on axis of symmetry of the arrangement caused by electrons from hollow cathode. Ions left behind in this region drift back into the hollow cathode, forming a positive space charge (virtual anode), which will distort the static electric field inside hollow cathode. This makes the electron production rate greater than the loss rate in the hollow cathode and the gap between cathode and anode. As a result, low resistance plasma is established and breakdown occurs eventually.

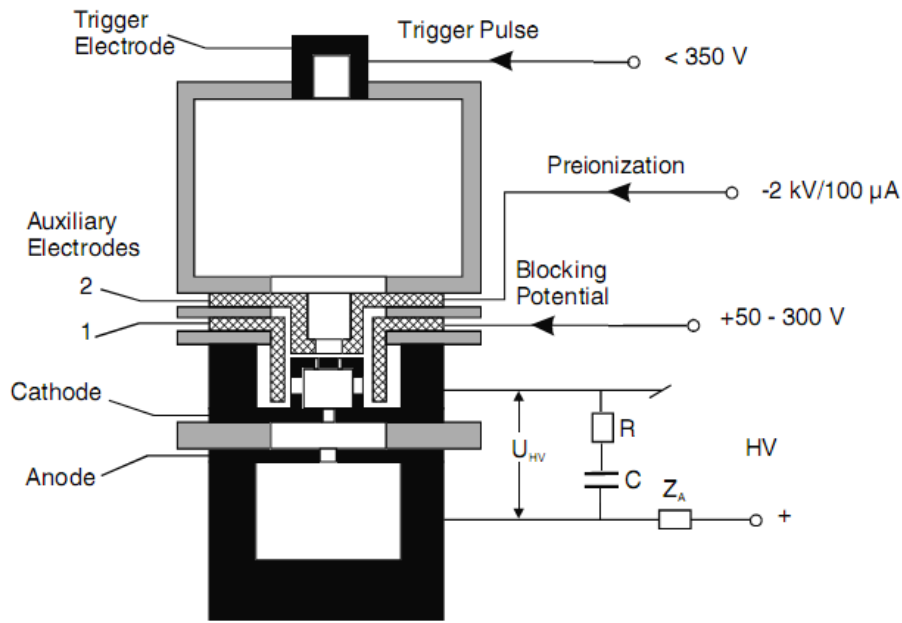


Figure 2.12 Cross sectional view of an electrical triggered pseudospark switch

As an example, the cross sectional view of one of the electrical pulse triggered pseudospark switch is shown in Figure 2.12. As seen in the figure, the switch consists of a pair of specially shaped anode and cathode and another electrode set for preionization. A low-current glow discharge ($I < 1\text{ mA}$) starting from auxiliary electrode-2 provides a weak ionization inside

the trigger section. To trigger the switch, a pulse discharge is generated ($I < 1$ A) by applying a negative pulse of 3 kV to the trigger electrode. When triggering takes place at cathode, charge carrier injection causes formation of a positive space charge within the hollow cathode. Couple of tens of nanoseconds later superemissive cathode phase starts by a change in electron emission mechanism to field enhanced thermionic electron emission. This provides a self-heated cathode process without any external heating. During this phase, discharge expands radially between the cathode and the anode gap. High peak currents are due to this phase of pseudospark discharges [6].

The time of switch establishment and the final switch impedance value are depended greatly on cathode materials. The delay and jitter of breakdown also depend on the number of initial electrons in the hollow cathode. There are several methods to create initials electrons. A jitter of less than 10ns and a delay of 0.5 μ s have been realized by the method of pulsed glow discharge [6].

Using hydrogen as filling gas, a maximum hold-off voltage for an one-gap system can be up to approximately 40 kV. Pseudospark switch of 20 kA switch current are commercially available as well [6]. It is possible to use even higher voltages if it works at very low pressure. However, the negative aspect is that it may reduce lifetime of the switch because of enhanced erosions of the electrodes.

2.4 Triggering Mechanisms

In order to trigger switches reliably, 10^9 to 10^{10} electrons are necessary inside the hollow cathode. There are three main triggering methods: Pulsed low-current glow discharge, surface discharge triggering, and optical triggering.

2.4.1 Pulsed Low-Current Glow Discharge:

In fact, a typical example for this trigger method has been mentioned in Figure 2.12, which is used to explain how pseudospark switch works. Figure 2.13 shows another example of pseudospark switch using pulsed glow discharge as its trigger method. A negative dc voltage applied to the trigger electrode sustains a hollow cathode discharge with the cathode of the main gap acting as an anode. The switch is triggered by a negative high-voltage pulse on the trigger electrode [8].

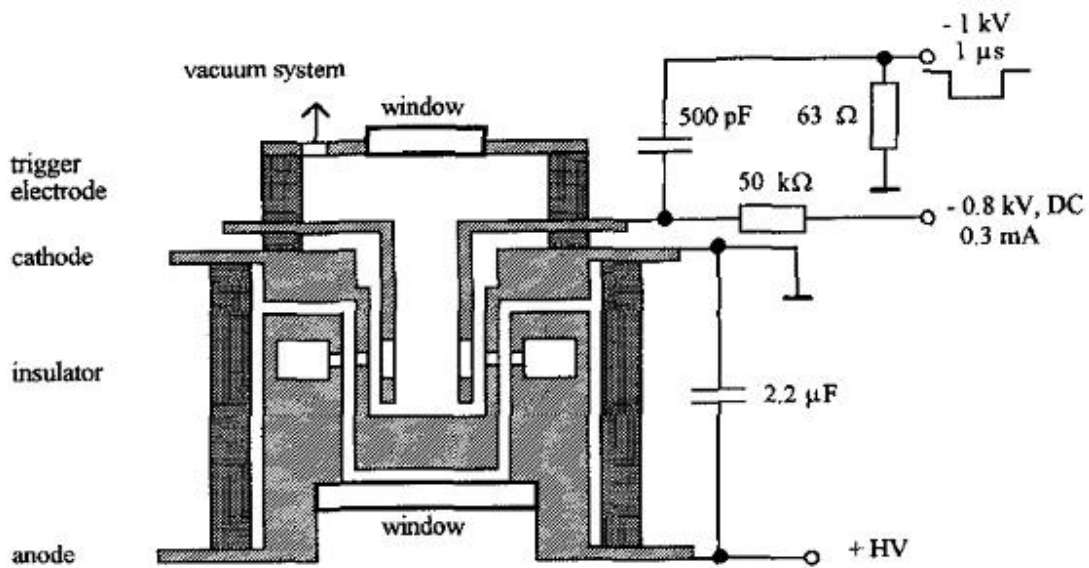
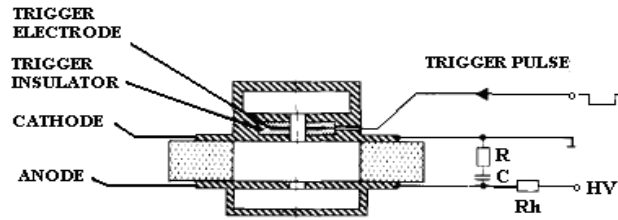


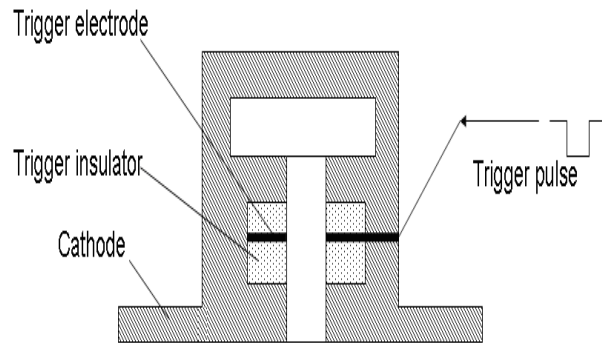
Figure 2.13 Schematic drawing of pseudospark switch with pulsed glow discharge trigger [8]

2.4.2 Surface Discharge Triggering:

The basic principle of surface discharge triggering is to take advantage of the electrons emitted from an insulator surface. Figure 2.14 shows a typical schematic drawing of pseudospark switch with surface discharge triggering.



a



b

Figure 2.14 (a) Schematic drawing of pseudospark switch triggered by surface discharge (b) enlarge view of the trigger electrode [9]

A trigger electrode is embedded between two insulator discs, and the electrode is inserted into the hollow cathode region of the main switch. To obtain electrons, it is necessary to apply a high voltage pulse to the trigger electrode. Moreover, it is important to have such kind of insulators that have low breakdown voltages and long lifetimes. Normally, surface discharge triggering creates high peak currents, which limit its repeatability. [10]

2.4.3 Optical Triggering

Backlighted thyatron (BLT), a new thyatron-type switch, is an optically triggered version of the pseudospark switch. The BLTs use unfocused light to initiate the discharge through

photoemission. This is ordinarily impossible with a high-current switch, as it has not been possible to fabricate devices that have both photosensitive cathodes and have the cathode in a region where either the laser or arcing produce permanent cathode damages. The light is incident on the back of the cathode. Typical operating parameters are 10-50 Pa H₂ or He, 3-mm electrode separation, and a few mill joules of UV radiation. Over 35 kV hold-off voltage has been obtained, with circuit-limited dI/dt $\sim 4 \times 10^{11}$ A/s.

A simple geometry of a BLT can be seen in Figure 2.15. Optical triggering has been demonstrated 1) by using an unfocused laser (XeCl at 308 nm and KrCl at 222 nm) directly incident on the back of the cathode, 2) by a flashlamp, 3) by radiation from a spark generated in air, and 4) by coupling laser radiation into the BLT cathode area through an optical fiber [11]. The compact structure of the anode and cathode, as well as the pseudospark and BLT results, suggest that extremely high dI/dt should be possible. A two-gap construction achieved hold-off voltages in excess of 60 kV.

Optical triggering has several advantages: complete electrical isolation of trigger source, reliable low energy triggering and simple structure. Furthermore, ability to trigger using fiber-optics is useful for perfect synchronization of several switches in parallel or in series [12]. Recently, compact BLT switches are reported with 3mm aperture, currents up to 4 kA and hold-off voltages more than 20 kV [3].

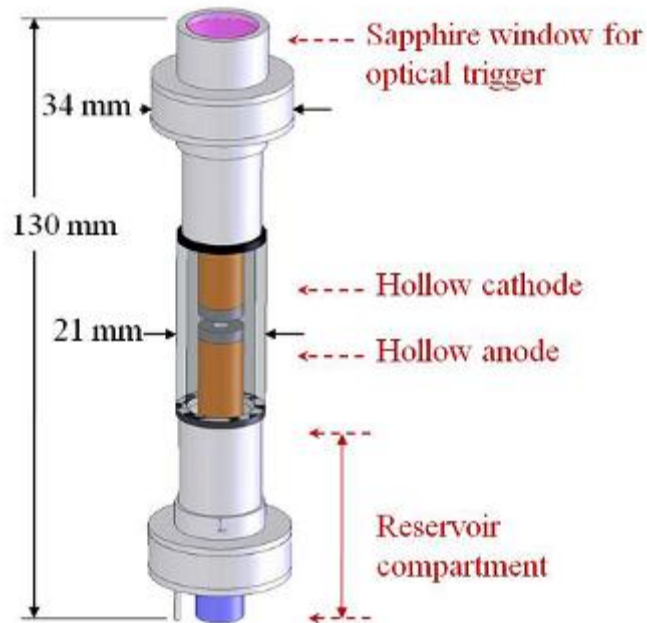


Figure 2.15 Compact BLT [13]

2.5 Field Emission Materials Literature Review

C. Liu reports that quasi-aligned aluminum nitride nano-cones on the silicon wafer display high field emission property [14]. These nano-cones are formed via the reaction between AlCl_3 vapor and NH_3/N_2 gas at the temperature ranging from 700% to 800% under nickel catalyst. The diameters of the tips of these cones are between 20 and 50 nm. It is revealed that the turn on voltage is around $12 \text{ V}/\mu\text{m}$. Based on the Fowler-Nordheim plot with a two-stage slope, the field enhancement factors are calculated to be about 400 and 1200 respectively.

It is reported by J. Y. Shim that amorphous carbon and diamond is able to emit electrons at low field intensity [15]. Amorphous carbon films are coated on Si emitters by helical resonator plasma enhanced chemical vapor deposition (HRPECVD). The data indicates that the field emission from the amorphous has a turn on voltage of about 185 V with distance of $150 \mu\text{m}$ between sample surfaces to the collector. The emission current of the emitters increases to 0.68

μA with increasing the applied voltage. For diamond coated Si emitters, the field emission occurs at a substantially low voltage of about 100 V in the 120 μm diamond emitters with a gap of 150 μm . The emission current from the diamond emitters is about 50 μA .

Polymethy methacrylate (PMMA) is reported to have a high field emission characteristic by W Y Huang [16]. Thin films of PMMA are formed by spin coating using chloroform solvent. Heavily doped-Si and metal (Al, Cu, et al) plate are used as the substrate. The lowest turn on voltage of PMMA is about 4 V/ μm , and the initial emission current increases from several nA to a few μA .

A low-threshold field emission from polished surface of metallic electrode which is covered by thin film of non-conjugated polymers such as: i) imide/ siloxane copolymer; ii) aryl-polycarbonate; iii) Nylon 66 are found [17]. The films are prepared by deposition of a solution on the polished Mo or Nb electrodes. Then films are heated in air at a constant temperature to remove the major part of the polymer solvent. A stable field emission at 4 V/ μm is observed, however for initial activation of the cathode the threshold field should be 2.5-3 times more than 4 V/ μm .

Deng Jicai reports that Nano-crystalline graphitic films have a high field emission characteristic [18]. Nano-crystalline graphitic films are synthesized from methane and hydrogen gas mixture directly on stainless steel plates by microwave plasma chemical vapor deposition (MWPCVD). Surface treatment of the samples, coated with metals (Ti), are performed by pulsed laser deposition (PLD) technique. The turn on electric field is measured to be about 4 V/ μm .

Field emission from selectively regrown GaN pyramids is measured by R.D. Underwood [19]. Hexagonal pyramids of GaN have been obtained by using atmospheric

pressure metalorganic chemical vapor deposition (MOCVD). The pyramid formation is the result of selective-area regrowth on a GaN epitaxial film. The pyramids are fabricated by the deposition of a dielectric mask to a GaN film, patterning of the mask, selective-area regrowth of the tips, and metallization of substrate contacts. The turn on electric field for GaN pyramids is about 3 V/ μm , and the maximum emission current of 81.7 μA is measured at 1100 V.

Field Emission Properties from Nano-clusters of Tungsten Oxide on Silicon Carbide is reported by S.Z.Deng [20]. Tungsten nano-clusters films are grown on silicon carbide substrate in a thermal evaporation process without using catalyst. The turn on field for obtaining the emission current densities of 10 $\mu\text{A}/\text{cm}^2$ is 11.5 V/ μm at temperature of 323 K, and decreases to 2.325 V/ μm at 543 K.

In addition to these field emitter materials, CNTs are also becoming candidate as excellent field emitters, which will be discussed in the following chapter.

CHAPTER 3

CARBON NANOTUBES

3.1 Carbon Nanotubes and Structure

For plasma switches, it is important to find a proper cold cathode material to be used as the “trigger electrode” to initiate the ionization processes. Since a trigger electrode provides the seed electrons to initiate the hollow cathode discharge, the materials of trigger electrode should have a high field emission rate.

Since the discovery in 1991 by Japanese researcher Iijima, carbon nanotubes have been attracting a wide attention, from both a fundamental point of view and for future applications [21]. Because of their electronic, optical, mechanical and chemical characteristics, they become one of the most promising nano-scale materials, and have been leading to implementation of practical and commercial products in such areas as high performance field effect transistors [22-27], single-electron transistors [28, 29], atomic force microscope tips[30], field emitters [31, 32], chemical/biochemical sensors [33-36].

Carbon nanotubes are members of the fullerene structural family. A fullerene is any molecule composed entirely of carbon, in the form of a hollow sphere, ellipsoid, or tube. The ends of a carbon nanotube are capped with a hemisphere of the buckyball structure. The reason why people call them nanotubes is because the diameter of a nanotube is on the order of a few

nanometers, while the length can be up to several millimeters. There are two main types of CNTs: single wall carbon nanotubes (SWCNTs) and multiwall carbon nanotubes (MWCNTs). They are also classified as random CNTs and Aligned CNTs.

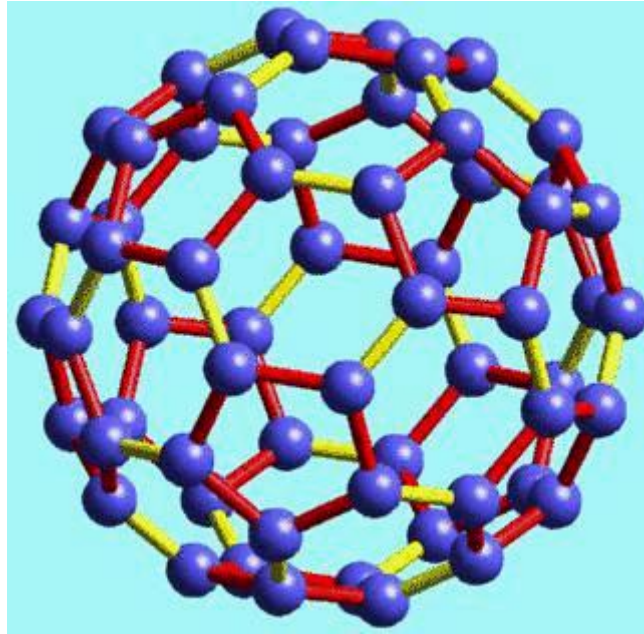


Figure 3.1 Buckyball structure [37]

There are many exotic structures of carbon nanotube exist: regular spheres, cones, tubes and others. The following will describe some of the most important and best-known structures of CNTs.

Single Wall Nanotubes (SWCNTs) are usually regarded as long wrapped graphene sheets. As they generally have a high length to diameter ratio of about 1000. The SWCNTs can be considered as nearly one-dimensional structures.

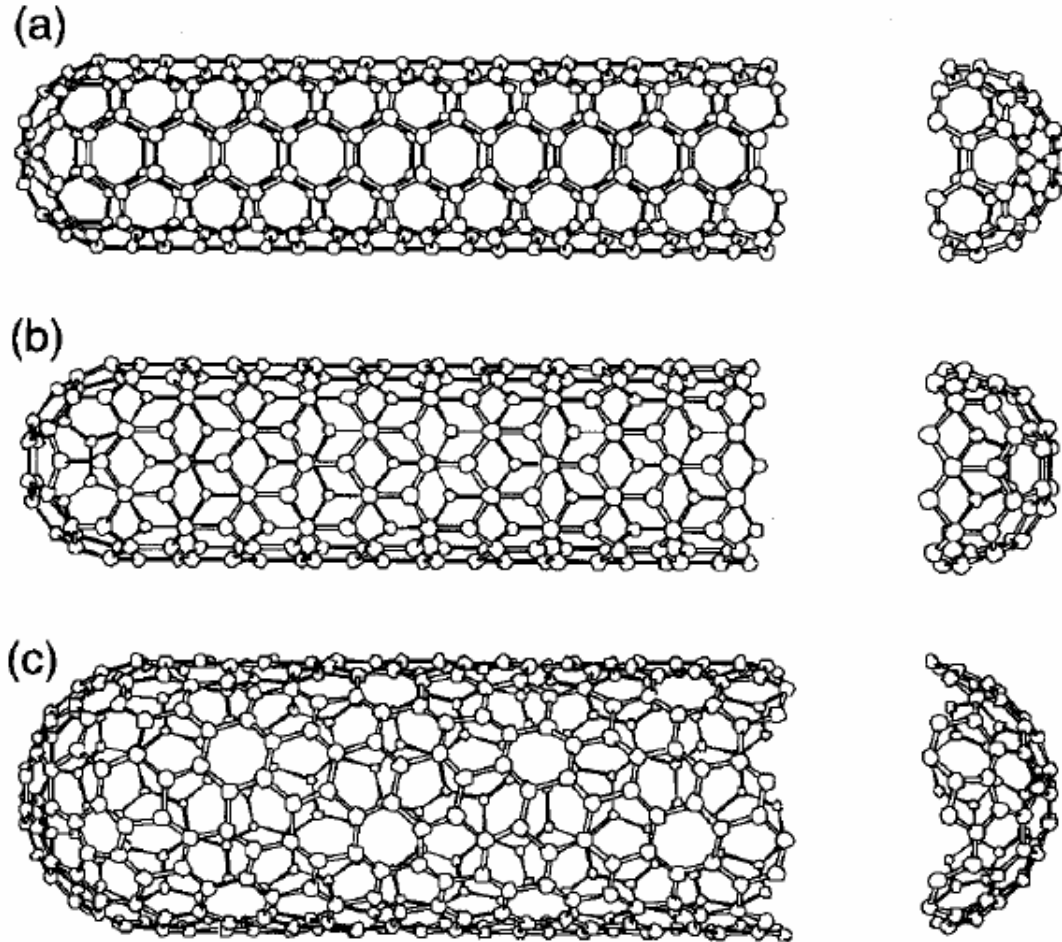


Figure 3.2 Classification of CNTs: (a) armchair, (b) zigzag, and (c) chiral nanotubes [38]

As shown in Figure 3.2, SWCNTs consist of two separate parts, which have different physical and chemical properties from each other. The first is the sidewall of the tube and the second is the end cap of the tube. The end cap structure is almost the same to a smaller fullerene, such as a buckyball structure. The end cap structures are formed by C-atoms placed in hexagons and pentagons. The combination of a pentagon and five surrounding hexagons can form the desired curvature of the surface to enclose a volume.

The other structure of SWNT is called cylinder. It is obtained when a certain size of graphene sheet is wrapped in a certain direction. The result is cylindrical symmetric structure.

There are two atoms in the graphene sheet, one of which serves the role as origin. The sheet is kept being rolled until the two atoms coincide. Further explanation of this structure is given in [39].

MultiWall Carbon Nanotubes (MWCNTs) can be considered as a collection of concentric SWCNTs with different diameters. Typical sizes for MWNTs are such that the inner diameter is approximately 1-3 nm and an outer diameter is approximately 10 nm. The length and diameter of these structures are quite different from those of SWCNTs and thus their properties are very different as well as showed in Figure 3.3.

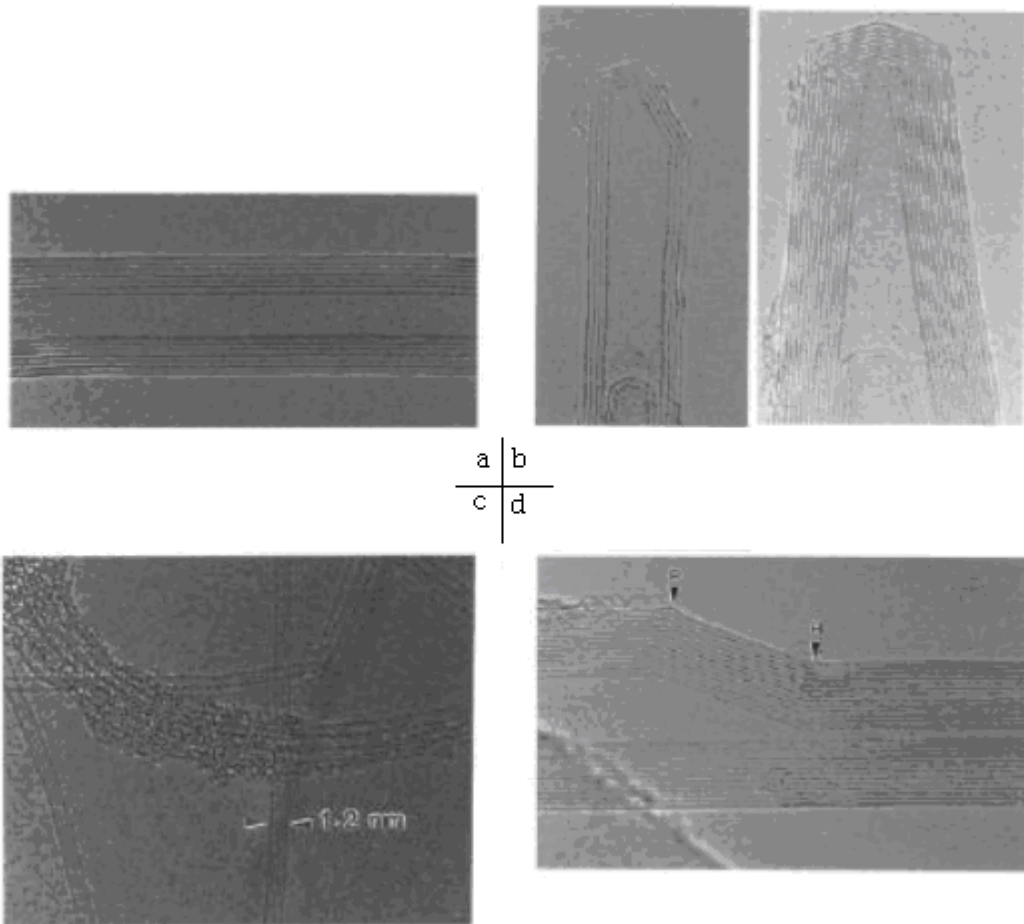


Figure 3.3 Different Structures of MWCNTs, (a): Cross-section of a MWCNT the different walls are obvious, they are separated by 0.34nm. (b): Symmetrical or non-symmetrical cone shaped end caps

of MWCNTs. (c): A SWCNT with a diameter of 1 to 2 nm and a bundle of SWCNTs covered with amorphous carbon. (d): A MWCNT with defects. In point P a pentagon defect and in point H a heptagon defect [40].

3.2 Properties of Carbon Nanotubes

Carbon nanotubes' nearly one dimensional structure determines their electronic, molecular and structural properties. Three of the most important properties of CNTs are chemical reactivity, electrical conductivity and mechanical strength are explained below.

Chemical reactivity [40]: Compared with a graphene sheet, the chemical reactivity of a CNT is increased as a direct result of the curvature of the CNT surface. Carbon nanotube reactivity is related to the pi-orbital mismatch directly as a result of an increased curvature. Therefore, there must be distinction between the sidewall and the end cap of a nanotube. Covalent chemical modification of either sidewalls or end caps has shown to be possible. Direct investigation of chemical modifications on nanotube behavior is difficult because so for the crude nanotube samples are not pure enough to allow investigations.

Electrical conductivity: carbon nanotubes with a small diameter can be either metallic or semi-conducting, depending on their chiral vector, which is defined as the vector pointing from one atom towards the other. The different conducting properties are results of their specific molecular structure with a different band structure and thus a different band gap. The differences in conductivity can easily be derived from the graphene sheet properties [41]. The resistance of conduction is determined by quantum mechanical aspects and was proved to be independent of the nanotubes length [42]. For more general information on electron conductivity is referred to a report by Ajayan and Ebbesen [43].

Mechanical strength: Carbon nanotubes have a very large Young modulus in their axial direction. The nanotubes as a whole are very flexible due to their great length. Therefore, these compounds are potentially suitable for future applications in composite materials which need anisotropic properties [44].

3.3 Synthesis of CNTs

3.3.1 Growth Mechanism

There are many different methods to grow CNTs, and in most of those the generation of free carbon atoms and the precipitation of dissolved carbon from catalyst particles are involved in the CNTs growth processes. The growth is finished when the catalyst particle is “poisoned” by the impurities or the stable metal carbide is formed. The precise mechanism of the formation of carbon nanotubes is still not clear. However, it is commonly believed that there are three main steps during the growth of CNTs. As shown in Figure 3.4, the fundamental steps are: (1) metal catalyst particles are formed, (2) free carbon atoms diffuse into the surface of the catalyst particles and form metastable carbide particles under high temperature, (3) Rod-shaped carbon tubes grow out of the catalyst particles rapidly. Depending on the interaction between the catalyst particles and the substrate, the catalyst particles may stay on the supporting substrate or leave the substrate.

Generally, Carbon nanotubes are produced by three main methods, laser ablation (Figure 3.6), arc discharge (Figure 3.5), and chemical vapor deposition (CVD). In the laser ablation technique, a high power laser beam impinges on a volume of carbon containing feed gas (methane or carbon monoxide). Meanwhile, laser ablation produces a small number of clean nanotubes. In arc discharge method, a vapour is created by an arc discharge, which occurs

between two carbon electrodes with or without catalyst. Nanotubes selfassemble from the resulting carbon vapors. In CVD method, the furnace is heated at a temperature of 600 -1000°C to decompose the gas, supplying carbon atoms for the CNTs growth. It is commonly believed that CVD can produce good MWCNTs but poor quality SWCNTs. The SWCNTs created by CVD have a large diameter range, which can be hardly controlled. But on the other hand, this method is easy to scale up, which favors commercial production [45].

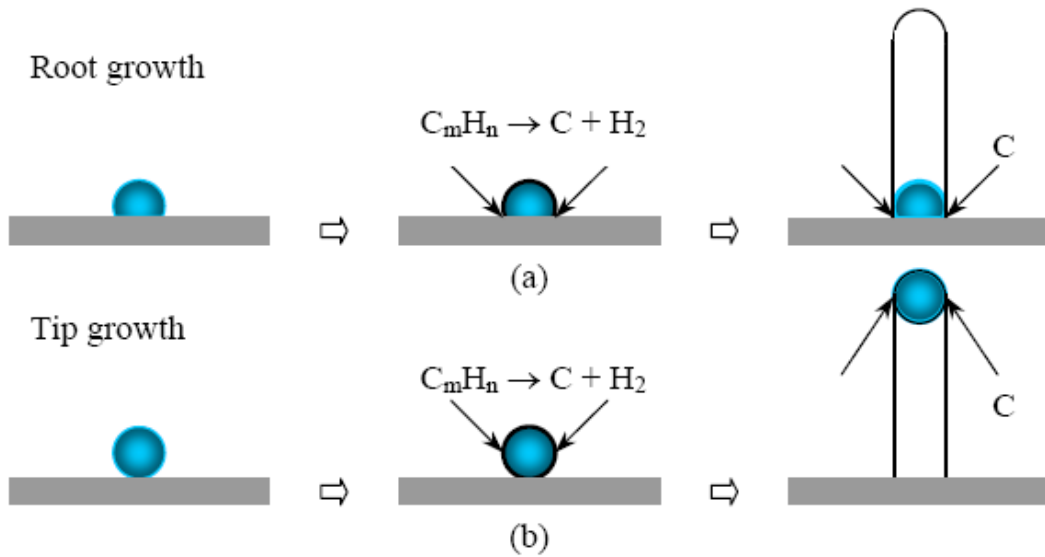


Figure 3.4 Schematics of the growth mechanism: (a) root growth and (b) tip growth [45]

3.3.2 Arc Discharge Method

It is very convenient to use carbon arc to generate a variety of carbon materials because it creates high temperature plasma, which has been used to produce CNTs, whiskers, soot, and fullerenes. The DC-arc method is preferred and becomes a commonly applied method for synthesizing MWCNTs. In order to produce high yield of MWCNTs, the conditions have to be carefully controlled [46].

Figure 3.5 shows the schematic drawing of a carbon arc apparatus. In this setup, both DC and AC power sources can be used. On the left-hand side is a short black negative electrode, where the deposit forms, and on the right-hand side is a long positive electrode that is consumed in the arc. The arc is generated between these two pure graphite electrodes. The position of the latter can be adjusted manually from outside the reactor in order to maintain a proper spacing between the electrodes to further keep the discharge stable, which can be monitored by measuring the

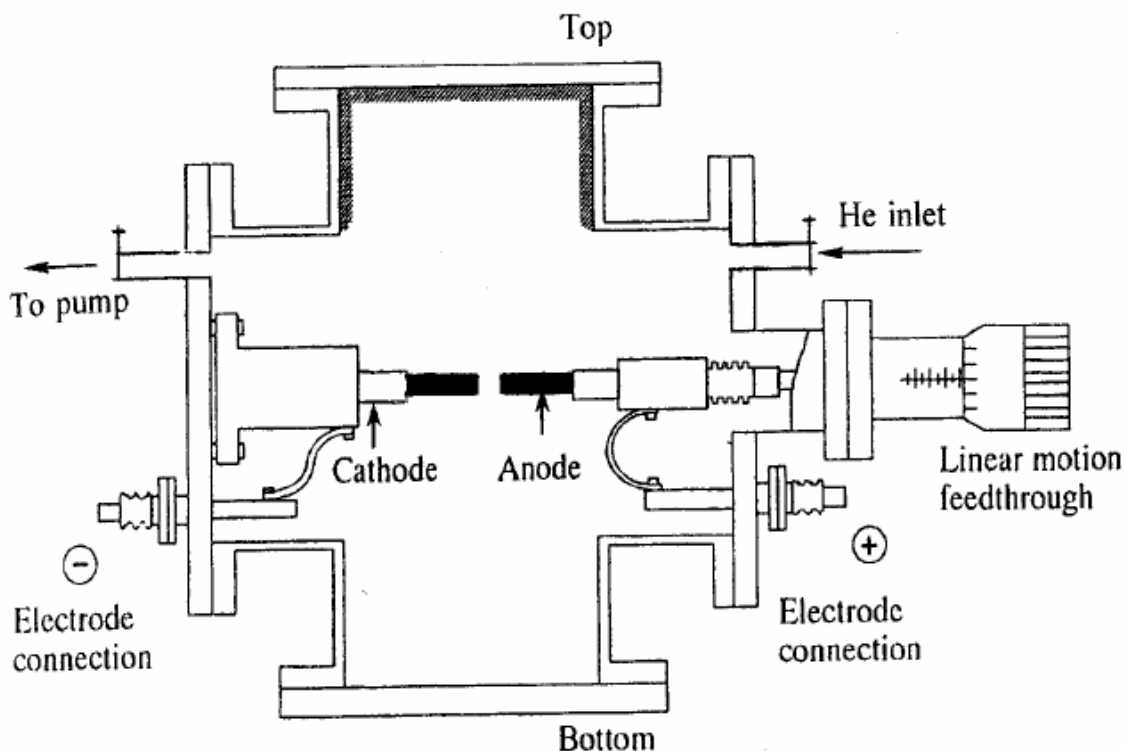


Figure 3.5 Schematic diagram of the arc apparatus [45]

discharge current. Typically, Helium is used in the chamber due to its low ionization potential. Since plasma is necessary, the type and pressure of the gas surrounding the arc becomes critical. It is common to use DC voltage of 20 V and gas pressure of 500 Torr, respectively. As soon as the arc is generated, current begins to flow resulting in a plasma with a temperature up to 3700°C. It has been reported that the lower the current is, the better the yield of CNTs can be gained [47].

3.3.3 Laser Ablation Method

Carbon nanotubes can also be synthesized by laser vaporization apparatus with an ablated pure graphite target located in an oven. It is reported that closed-ended MWCNTs can be produced in the gas phase through homogeneous carbon-vapor condensation in a helium/or hot argon atmosphere [48]. MWCNTs synthesized by laser ablation are relatively short (~300 nm), compared to those synthesized by arc discharge. The number of layers deposited by laser ablation can range between 4 and 24. The inner diameter varies from 1.5 to 3.5 nm. The quality and yield of MWCNTs degrade as oven temperature decreases.

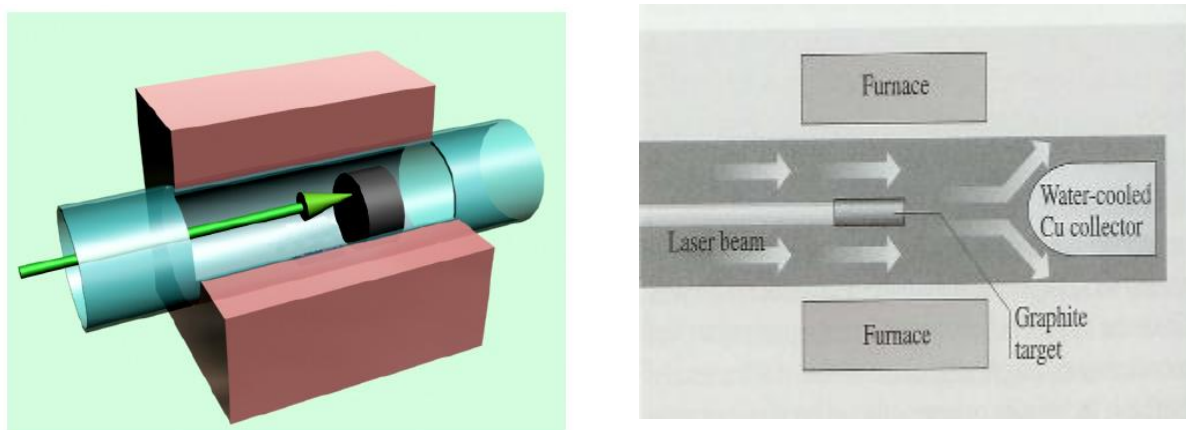


Figure 3.6 Schematics of experimental setup of laser ablation technique [49]

Laser system for synthesizing carbon nanotubes can be operated in either pulsed mode or continuous mode. Figure 3.6 shows a schematic diagram of the traditional laser ablation system for carbon nanotubes growth [49]. A graphite target is loaded in the center of a quartz tube furnace that is filled with inert gas. The operating temperature is set at 1200°C. The laser beam is focused at the graphite target in order to vaporize and sublime the graphite by uniformly bombarding its

surface. The carbon species swept by a flow of neutral gas are thereafter coated as soot in different regimes: (1) on the conical water-cooled copper collector, (2) on the wall of quartz tube, and (3) on the backside of the target [49].

3.3.4 Chemical Vapor Deposition

In order to use carbon nanotubes for nanoelectronics, field emission applications require more accurately controllable growth on the patterned substrate at reasonable rates. Chemical vapor deposition (CVD) can satisfy this requirement. One CVD method for CNTs growth is thermal chemical vapor deposition, in which a conventional heat source such as resistive or inductive heater, or infrared (IR) lamp is used to heat the environment in a furnace. Another CVD method is called the plasma-enhanced chemical vapor deposition (PECVD), in which the plasma source is used to create a glow discharge which contains desirable radicals, electrons, and ions.

DC, RF (13.56 MHz), or microwave (2.45 GHz) sources can be used to generate plasma (Figure 3.7) [50]. A plasma reactor consists of a pair of electrodes in a chamber with one electrode grounded and the other one connected to a power supply. When applying a negative bias (>300 V) on the cathode, a breakdown of feed gas occurs. The resulting glow discharge is composed of positive and negative ions, electrons, atoms, and radicals. The distance between these two electrodes is determined by Paschen law, $Pd = \text{constant}$, where P is the pressure and d is the distance between two electrodes. This means that in order to sustain the discharge, electrodes have to be pulled away further as the pressure is decreased.

The electrode holding the substrate is heated by a source to elevate the substrate temperature to a desired growth temperature, and to increase the nucleation density. Precursor dissociation in the gas phase is not necessary in carbon nanotube growth by CVD. Dissociation,

however, at the catalytic particle surface appears to be the critical point for nanotube growth.

To prevent excessive production of amorphous carbon, it is necessary to keep the growth temperature below the pyrolysis temperature of the particular hydrocarbon [50]. Since the plasma can ionize the hydrocarbon gases which create lots of reactive radicals, pure hydrocarbon feed gas in plasma reactors may create substantial amorphous carbon deposition. It is necessary to dilute the hydrocarbon gases with argon, hydrogen, or ammonia. Typical reacting pressure of nanotube deposition is in a range from 1 to 20 Torr.

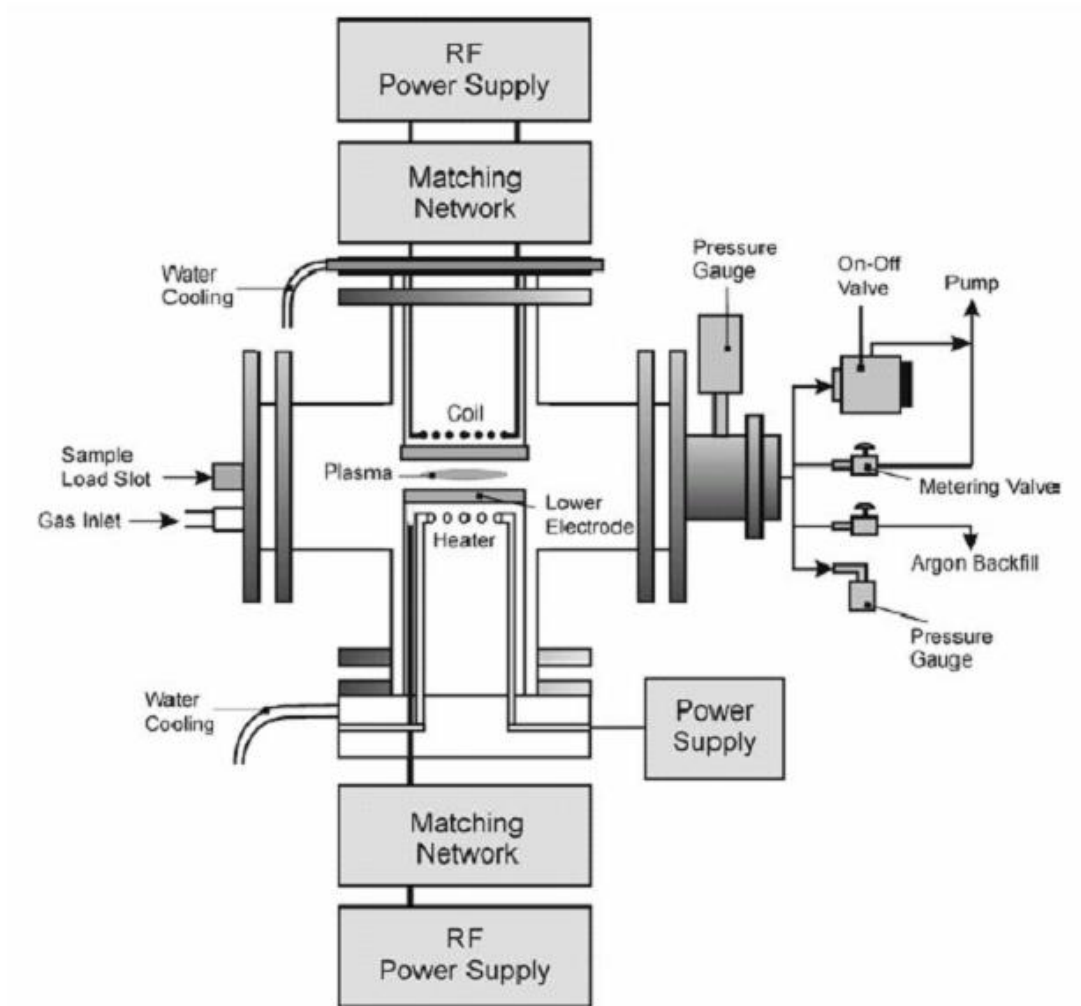


Figure 3.7: Schematic diagram of a PECVD setup for carbon nanotubes growth [50]

Compared to other methods, PECVD allows nanotubes to grow at a much lower temperature, which makes it appealing for integrating carbon nanotubes into the applications of semiconductor device fabrication. Furthermore, the local electrical field generated between the substrate holder and plasma provides nanotubes to grow extremely vertical with high density. PECVD is more capable of producing more vertically aligned carbon nanotubes structure growth than thermal CVD does. Whereas any marginal alignment nanotubes observed in thermal CVD samples are resulted from crowding effect, nanotubes supporting each other by van der Waals attraction. Thus, individual, free-standing and vertically oriented structures are obtained possibly by using PECVD.

CHAPTER 4

FIELD EMISSION EXPERIMENT

4.1 Research Objective

As stated earlier, the primary objective of this work is to find appropriate trigger electrode materials to create seed electron emission for pseudospark switches, the advantages of using this field emission triggering is that the switch can be designed compact and would be easy to construct.

In order to achieve the objective, a series of experiments measuring field emission characteristics of different materials are conducted. A vacuum chamber equipped with ports to place samples, electrodes and pressure gauges is used in the experiment. The pressure of the background gas (Helium or air) is varied from 10^{-6} Torr to 1 Torr for each experiment set. As a matter of factor, the field emission of there materials in the pressure ranging from 10 mTorr to 1 Torr is relatively important, since the pseudospark switches are normally operated in this pressure range. Mostly, the field emission characteristics of materials are measured in high vacuum of below 10^{-6} Torr.

In addition, the comparison of SEM images of the samples before and after the experiments is presented to demonstrate that these samples can be operated under these various low pressure conditions, without any damage, especially in the pressure higher than high

vacuum.

The materials tested in this work include SWCNT, MWCNT, Nanocrystalline Diamond, Nanorod ZnO and Oxygen-free Copper. All of their field emission characteristics are shown in the following sections.

4.2 Experiment Setup

The samples are loaded into a high vacuum chamber in which the electron field emission characterizations of the samples are measured. The chamber is first pumped by a Mechanical pump to the pressure of several tens of mTorr, then the turbomolecular pump is turned on to pump the whole chamber to the pressure of 1×10^{-6} Torr. Thus, by using mechanical and turbomolecular pump, the pressure of the chamber can be set at range from 1×10^{-6} Torr to several Torr.

The sample holder and Collector are separated by a glass cover sheet with a thickness of 250 μ m with an opening area of 0.1 cm^2 , which allows the electrons to be emitted from the sample and collected by anode. The anode collector is made of aluminum, and the cathode sample holder is made of copper. Samples need to be stuck to holder by double sided adhesive copper conducting tapes in this experiment.

A digital dc power supply (Stanford Research Systems PS235, with maximum output voltage of 5 kV and maximum output current of 2 mA) is used to apply a voltage between the anode and cathode. A Keithley 485 picoammeter is used to measure the emission current. By using a GPIB card, the power supply and the ammeter are connected to a desktop computer, by which voltage and current are recorded for further evaluations (Figure 4.1).

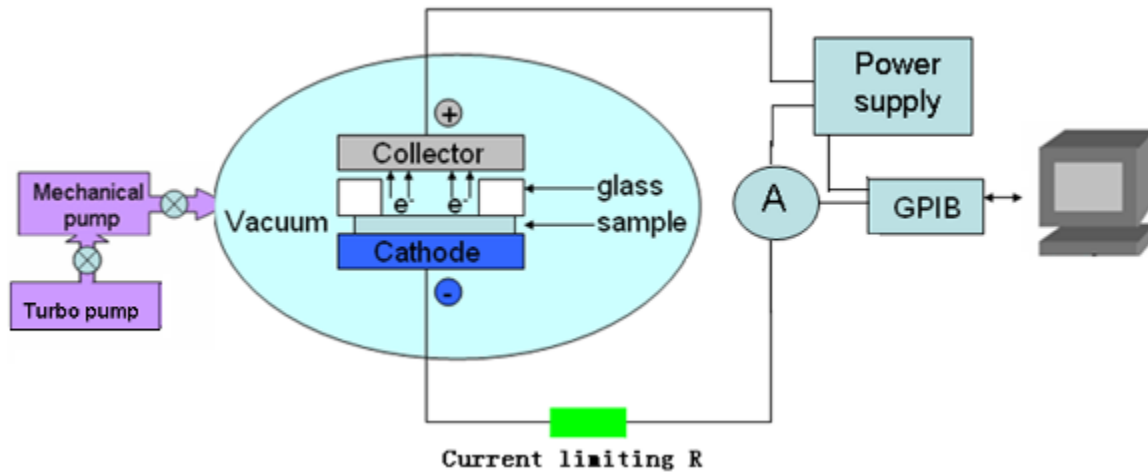


Figure 4.1 Circuit diagram of field emission intensity measurement set-up

For each measurement the applied voltage increased from 0 volt to a certain value (until a saturation current level is reached) with increments of 5 to 10 V, and then decreased from the peak value back to 0 Volt. Picoammeter measured and saved the emission current every time when the apply voltage steps up or down.

For data collection and control of the power supply and picoammeter, Labview program is used. By setting the parameters in Labview code, the step voltage, peak voltage and the step time can be controlled. The typical step voltages are 5 and 10V, the step time is about 0.5s and the peak voltage varies depending on materials' field emission characteristic. With Equation

4.1, the electrical filed intensity E can be calculated, $E = \frac{U - jR}{d}$ where U is the applied voltage,

j is the current intensity, R is current limiting resistor which is in the order of $M\Omega$, d is the gap distance (equal to $250\ \mu\text{m}$).

The total number of electrons emitted from the samples' surface can be derived from the current measured by the pico-ammeter.

4.3 Field Emission Characteristics of CNTs

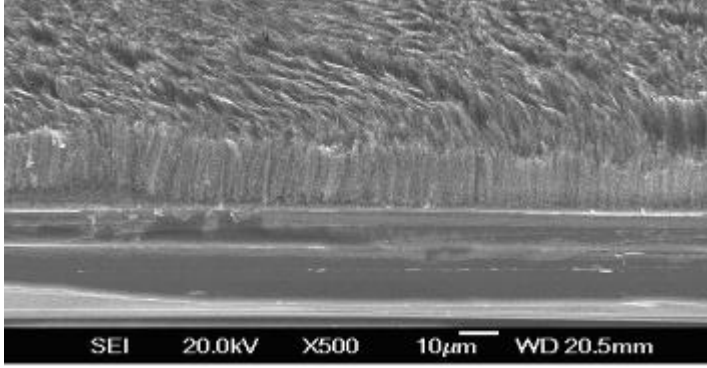
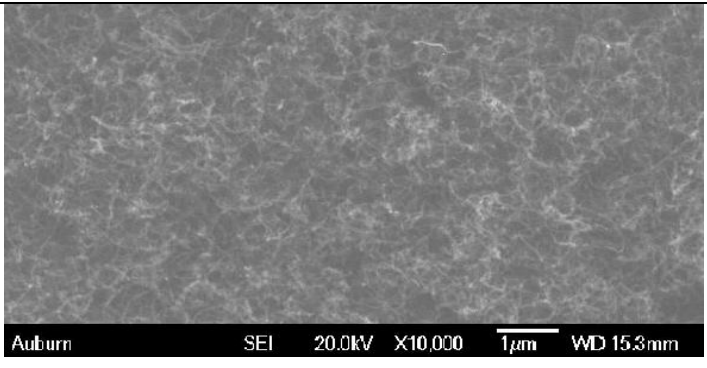
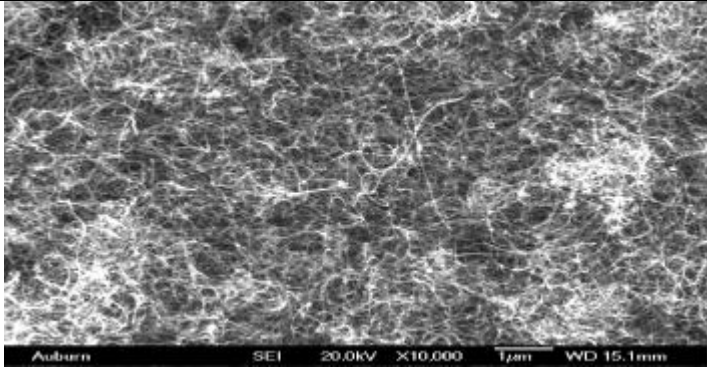
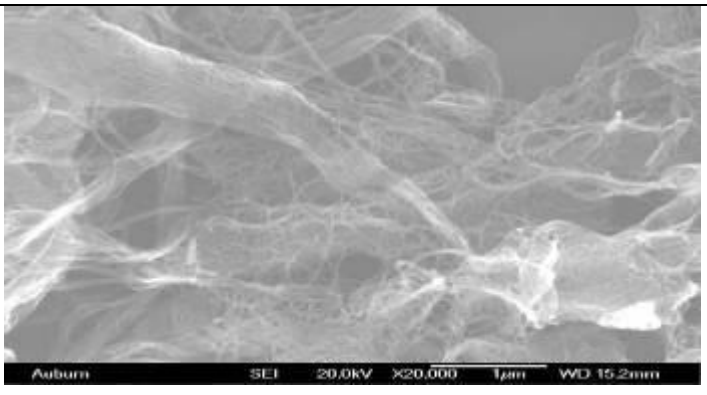
In this work, the electron emission characteristics of three different Carbon Nanotube samples, namely random MWCNT, Aligned MWCNT and random SWCNT, are measured and compared to each other. The field emission measurements are conducted under He and air background gasses and the comparison of the field emission characteristics under different background pressure and gas are shown. For these experiments, the SEM images of the samples before and after the measurements are recorded.

4.3.1 SEM Images of CNTs

Before Experiment

Figure 4.2 and Figure 4.3 are the SEM images of the aligned MWCNT. Figure 4.4 and Figure 4.5 show the SEM images of Random MWCNT and Random SWCNT respectively. These images are taken before the field emission experiment. The resolutions could be found in the figures. As we can see there are considerable differences among these three samples.

Table 4.1 SEM images of CNTs before experiment

	<p>Figure 4. 2 SEM image of Aligned MWCNT with a tilted angle of 20 degrees, 500 resolutions.</p>
	<p>Figure 4.3 SEM image of Aligned MWCNT, top view with resolutions of 10,000</p>
	<p>Figure 4.4 SEM image of Random MWCNT, top view with resolution of 10,000</p>
	<p>Figure 4.5 SEM image of Random SWCNT, top view with resolution of 20,000</p>

After Experiment

Table 4.2 SEM images of CNTs after experiment

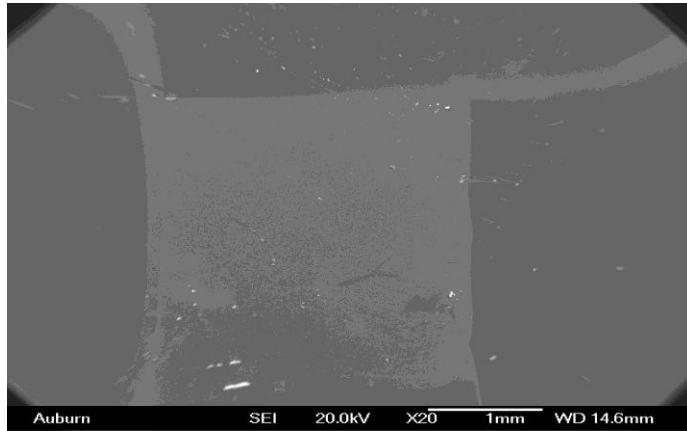


Figure 4.6 SEM image of the entire filed emission area of Random MWCNT , top view with resolution of 20

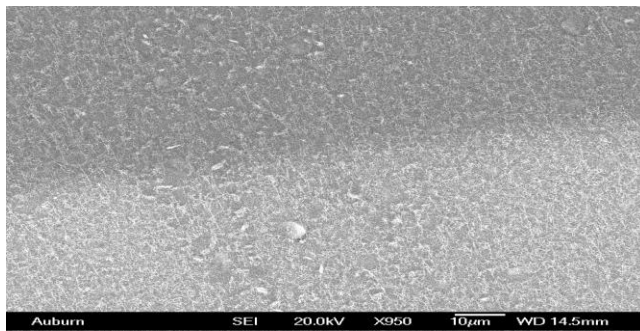


Figure 4.7 SEM image of the comparison between filed emission area (lower white part) and non-exposed area (upper dark part), Random MWCNT, top view with resolution of 950

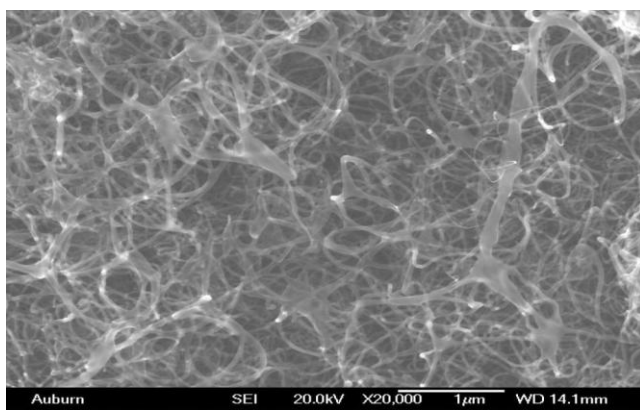


Figure 4.8 SEM image of Random SWCNT, top view with resolution of 20,000

Figure 4.6 shows the image of Random MWCNT sample after the experiments. The light colored area in the center is the region where the glass opening is, and therefore it is the area where the field emission took place. Compare to the color of non-field emission area, that of field emission area is whiter. Figure 4.7 shows the color difference more apparently in higher resolution. The upper dark part is the area that was shielded by the glass spacer and is the non-field emission area. The lower white part is where field emission occurred.

Figure 4.8 shows a SEM image of Random SWCNT after the field emission experiment, top view with resolution of 20,000. As we can see in the figure, there are some light points which are considered as the area where the electrons emitted. On the other hand, the integrities of the sample has not changed. The CNTs are still present and un-altered.

4.3.2 Field Emission Intensity

Field Emission Comparison in High Vacuum

Figure 4.9 shows field emission characteristics of these three CNT samples in high vacuum pressure of 10^{-6} Torr. As seen in the figure the turn on electric field strength (E_t) of Random SWCNT is about $0.4 \text{ V}/\mu\text{m}$, the lowest one among these materials. The second lowest turn on field is determined to be the Random MWCNT with $1.1 \text{ V}/\mu\text{m}$ and the largest turn on field is found to be for the Aligned MWCNT with $3.3 \text{ V}/\mu\text{m}$. The peak emission current of these three samples are about the same with approximately $1 \text{ mA}/\text{cm}^2$. Also as we can see, to obtain the peak emission current intensity, E needs to be $0.8 \text{ V}/\mu\text{m}$ for Random SWCNT, $2 \text{ V}/\mu\text{m}$ for Random MWCNT, and $4 \text{ V}/\mu\text{m}$ for Aligned MWCNT.

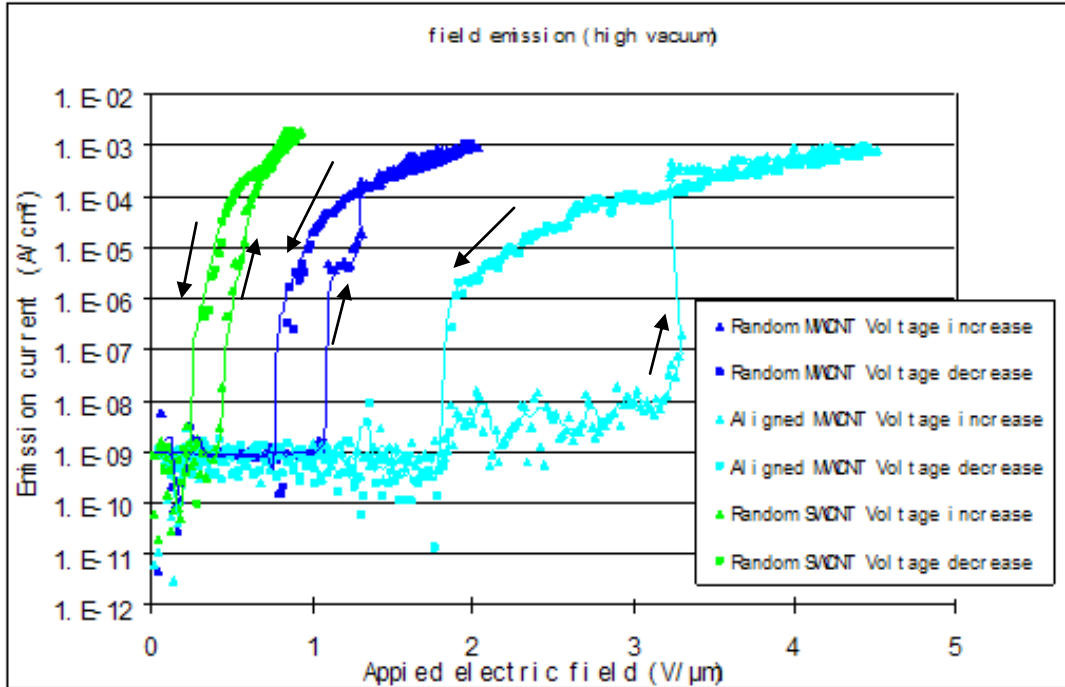


Figure 4.9 Field emission characteristics of three samples used in the experiments

Field Emission under Different Pressures

Figure 4.10, Figure 4.11, and Figure 4.12 represent the field emission characteristics of Random MWCNT, Aligned MWCNT, and Random SWCNT under different background pressures respectively. From these three figures it is easy to find that as the background pressure increases, E_t increases as well for all the samples studied. To get the same saturation emission current, the applied electric field needs to be larger at higher pressure than it is for the lower pressure. Although in high pressure, such as 1.0 Torr, the turn on field is higher than it is in lower pressure, it turns out that CNTs are able to emit a large amount of electrons without any damage to the samples in traditional plasma switch pressures.

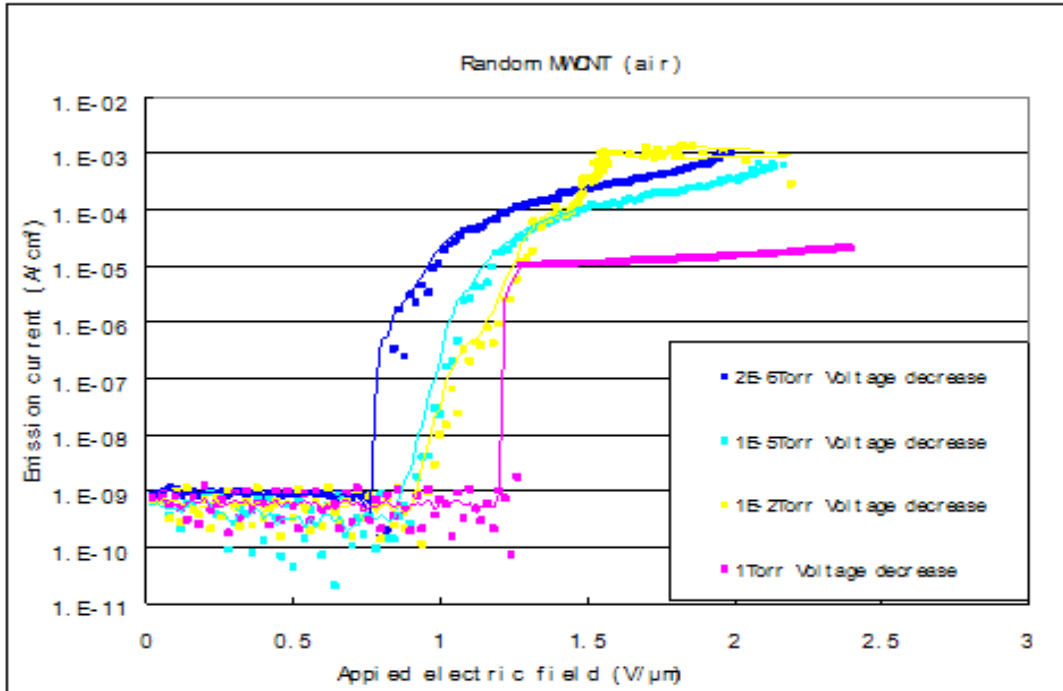


Figure 4.10 Field emission of Random MWCNT in different pressures of air

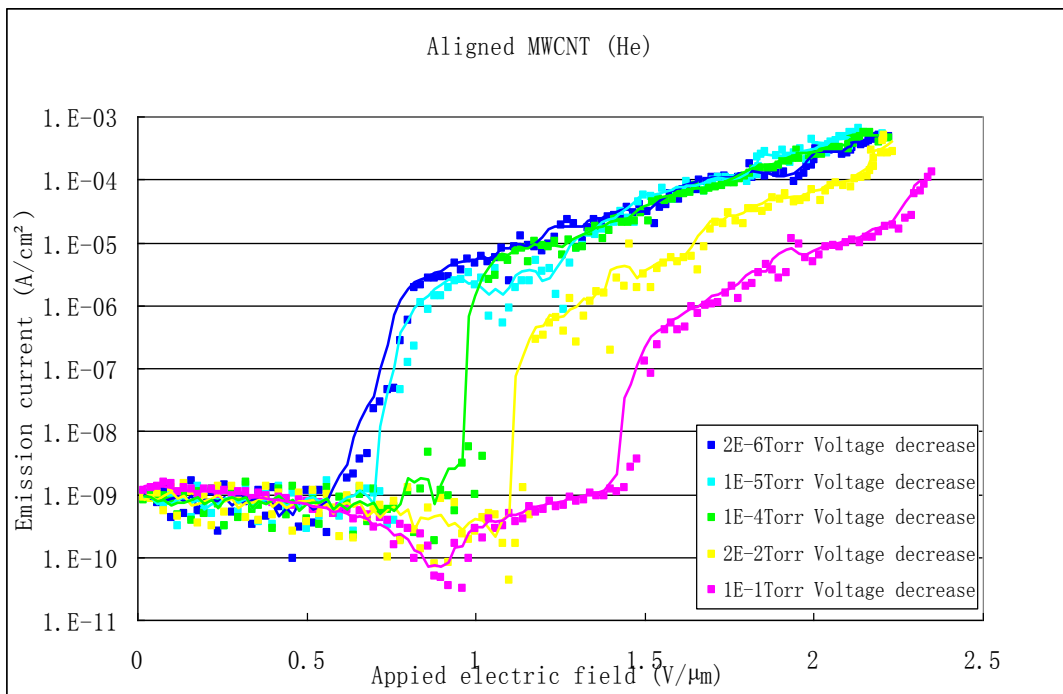


Figure 4.11 Field emission of Aligned MWCNT in different pressures of He

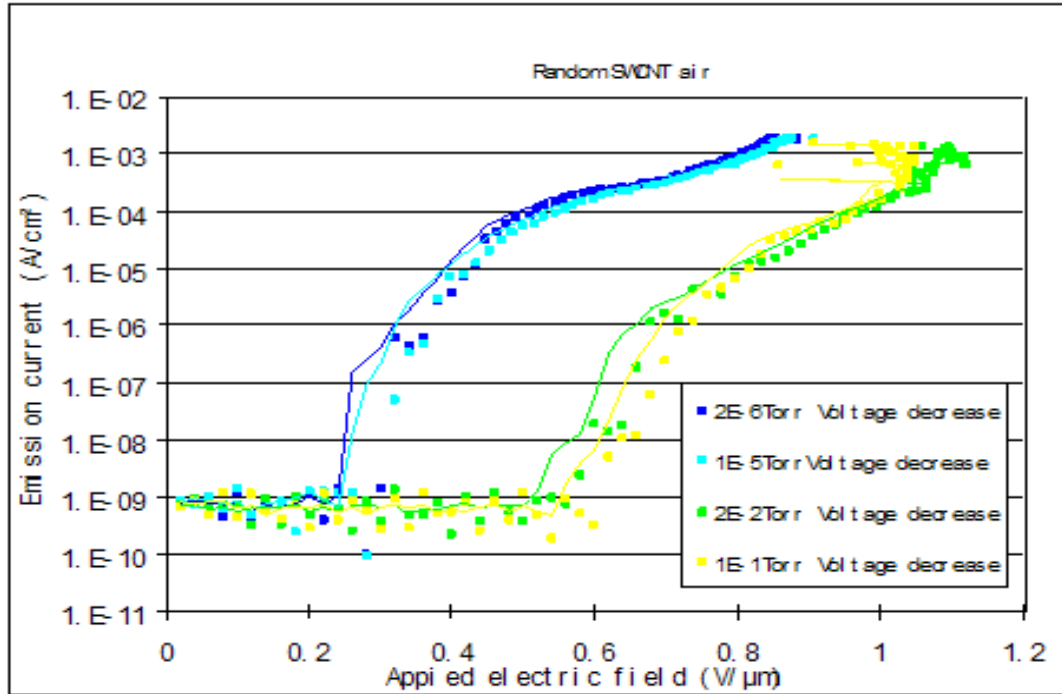


Figure 4.12 Field emission of Random SWCNT in different pressures of air

Field Emission Comparison in Air and He

The comparison of field emission characteristics of the SWCNT samples under two different background gases, namely air and Helium, is shown in Figure 4.13. It is seen in this figure that the turn on voltage in He is smaller for all the samples than it is in Air. In addition to it, the peak emission current in He is a slightly larger than the one observed when the background pressure is air. It should be noted that the traditionally used gas for pseudospark switches is hydrogen. However, helium is used in this work as the background pressure in the measurements. Because, it is a better gas to handle and its plasma characteristics are better understood.

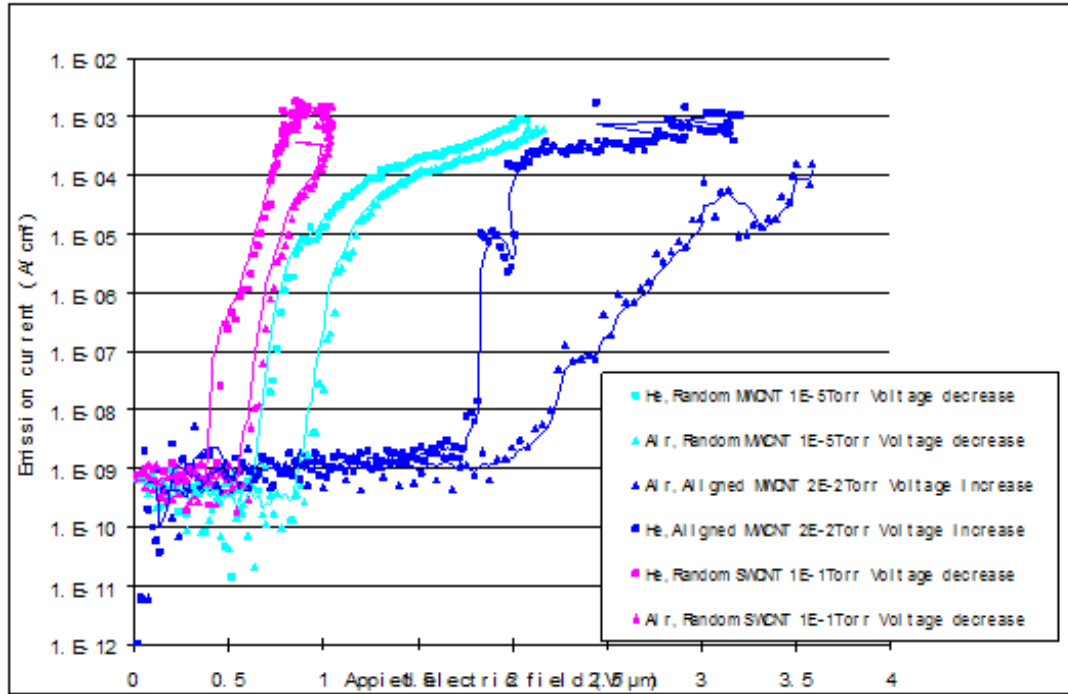


Figure 4.13 Comparison of samples' field emission in air and He

As a summary for CNTs, we see that CNTs have good field emission properties both in high and low vacuum. Therefore the CNTs could be applied to the plasma switch as a trigger material. As the pressure increase, usually the turn on electric field of CNTs increase, and the field emission saturation current density decreases. We also observe that Random SWCNT has better field emission characteristic than the others, since the turn on electric field is the lowest and the saturation current density is the highest. Among the random and aligned CNT, the aligned MWCNT's turn on electric field is the highest and the saturation current density is the lowest. On the other hand, the field emission characteristics of Random MWCNT are better than these of Aligned MWCNT. Compared to the samples in air, those in helium have better field emission characteristics, lower turn on electric field and higher field emission current density. This combined with having low turn on voltage at "high" pressure (i.e. 1 Torr pressure) may allow these materials to be used in plasma switch trigger electrode.

4.4 Field Emission of Zinc Oxide (ZnO)

The Zinc Oxide structure used in this work is nanorod, which is promising candidate as a new type of high-sensitivity ultraviolet (UV) photodetector due to its wide bandgap and large aspect ratio. In this study, single-crystalline ZnO nanorods are fabricated by thermal chemical vapor deposition (CVD) which is able to generate high density and high aspect ratio of uniformly growth ZnO nanostructure arrays. The ZnO nanorods used in this work were produced by Cheng An-Jen in Auburn University. [39]

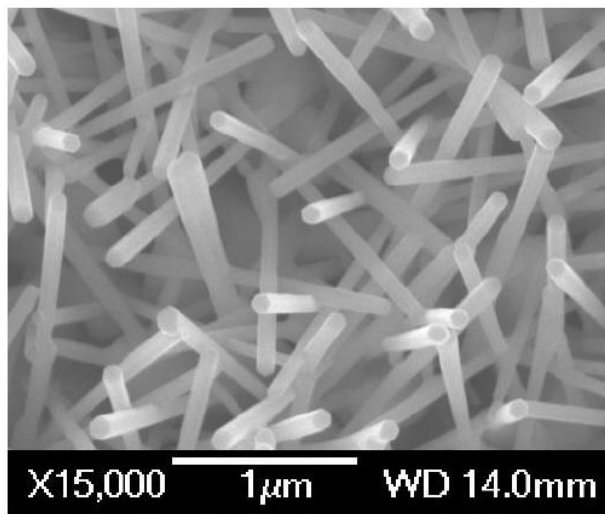


Figure 4.14 SEM images of ZnO sample surface with 15,000 resolution

Figure 4.14 shows the SEM image of ZnO nanorods in top view, sample surface with 15,000 solution.

The field emission intensity of ZnO is shown in Figure 4.15. The voltage between the gap is varied from 0 to 600 V, with 5 V steps. The pressure for these measurements is 1×10^{-6} Torr.

The current begins to increase drastically when the applied E field reaches $1.5 \text{ V}/\mu\text{m}$. From the plot, we can see that the peak emission current value is approximate $1 \times 10^{-3} \text{ A}/\text{cm}^2$.

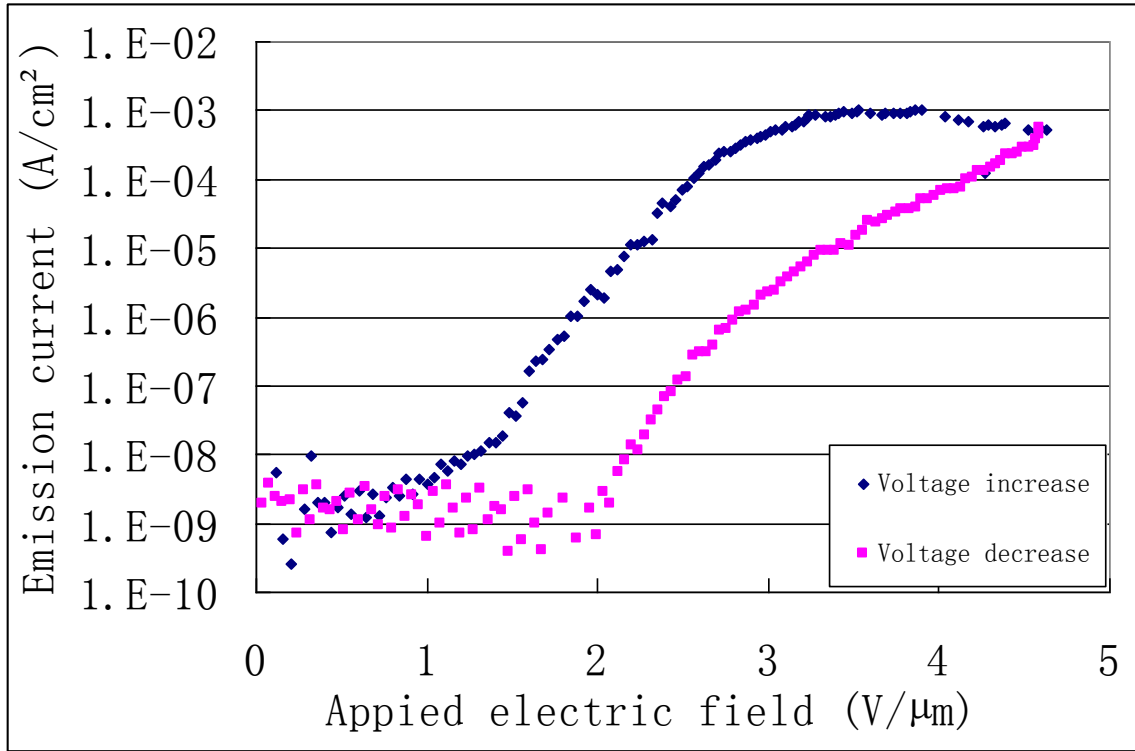


Figure 4.15 Field emission characteristic of ZnO nanorods at pressure of 10^{-6} Torr

The field emission intensity of ZnO nanorods at pressure of 2×10^{-2} Torr is shown in Figure 4.16. At this case, the field emission starts when the applied electric field is about $2.2 \text{ V}/\mu\text{m}$, which is a little bit larger than the one at lower pressure of 1×10^{-6} Torr. Additionally, the saturation current is less than $1 \times 10^{-4} \text{ A}/\text{cm}^2$.

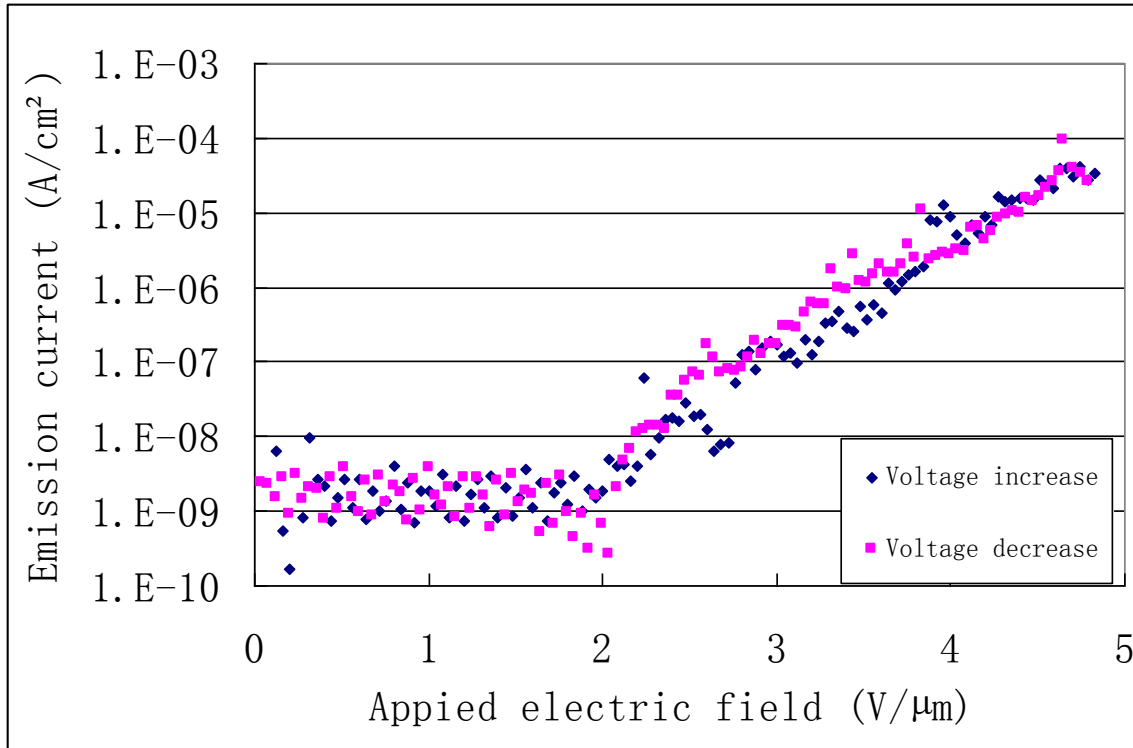


Figure 4.16 Field emission characteristic of ZnO nanorods at pressure of 2×10^{-2} Torr

4.5 Field Emission of Oxygen-free Copper

In this work, field emission intensity of oxygen-free copper (OFC) is measured. OFC generally refers to a group of wrought high conductivity copper alloys that have been electrolytically refined to reduce the level of oxygen in copper to .001% or below. According to our experiment, there is no electron emission when the surface of the CFC is smooth. Therefore, it is necessary to scratch the surface to form texturing on the surface. Once the surface no longer was smooth, the field emission from the OFC was measured. The following figure shows the SEM picture of the OFC with resolution of 2000.

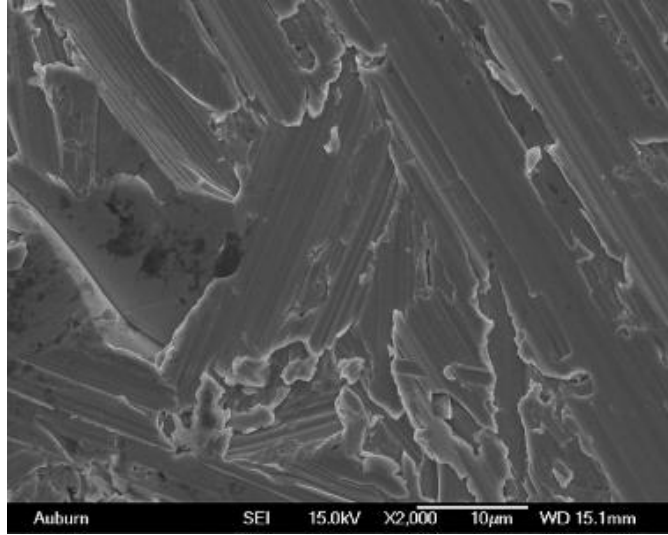


Figure 4.17 SEM images of oxygen-free copper surface with 15,000 resolution

Figure 4.18, Figure 4.19, Figure 4.20 show field emission intensity of OFC at pressure of 4×10^{-6} Torr, 1×10^{-5} Torr and 2×10^{-2} Torr, respectively.

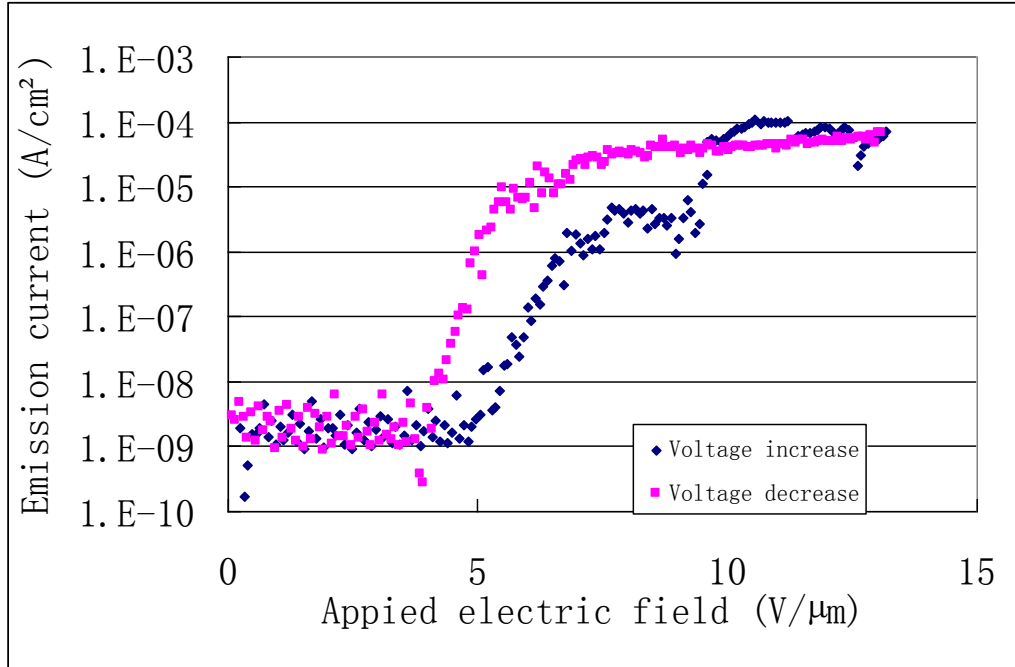


Figure 4.18 Field emission characteristic of Oxygen-free copper at pressure of 4×10^{-6} Torr

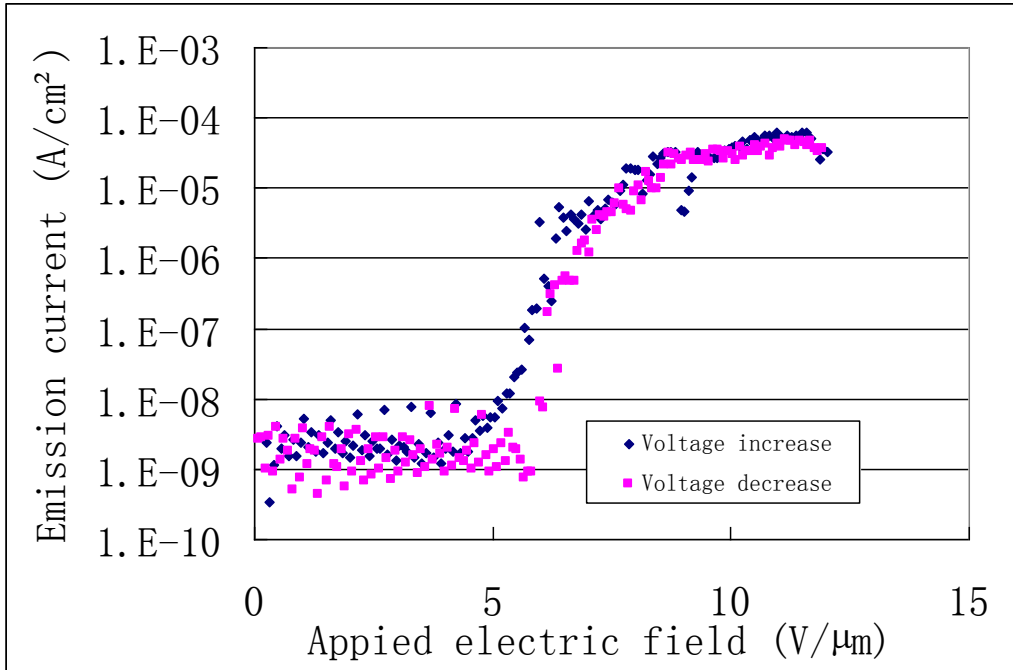


Figure 4.19 Field emission characteristic of Oxygen-free copper at pressure of 1×10^{-5} Torr

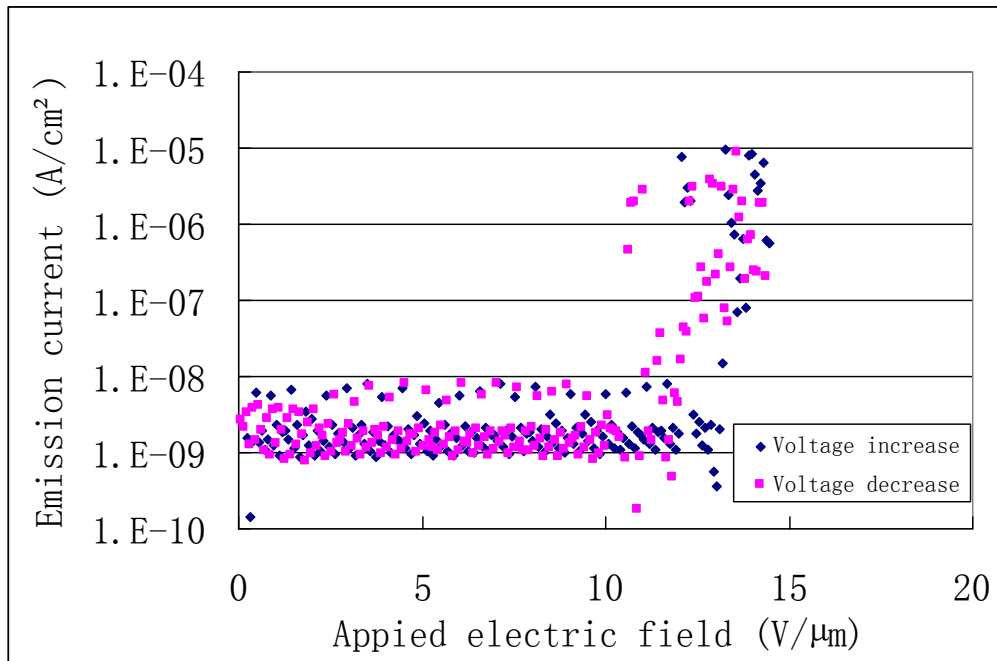


Figure 4.20 Field emission characteristic of Oxygen-free copper at pressure of 2×10^{-2} Torr

Under the pressure of high vacuum, Oxygen-free copper starts to emit electrons at

around $5 \text{ V}/\mu\text{m}$ and the saturation emission current can be up to $1 \times 10^{-4} \text{ A}/\text{cm}^2$. From Figure 4.20, we can see that under pressure of $2 \times 10^{-2} \text{ Torr}$, the field emission occurs at field intensity of about $12.5 \text{ V}/\mu\text{m}$, which is quite large compared to the previous one measured under high vacuum. Additionally, the maximum emission current can only reach up to $1 \times 10^{-5} \text{ A}/\text{cm}^2$. The reason why the field emission characteristics are different between high vacuum and low vacuum might be there is arc discharge or other discharges around the aluminum electrodes.

4.6 Field Emission of Nanocrystalline Diamond

Nanocrystalline diamond attracts a large number of interests due to its unique electrical and mechanical properties different from single crystal and polycrystalline diamonds. The smooth surface of nanocrystalline diamond makes it a good candidate for patterning other external structures onto as substrates, including surface acoustic wave (SAW) devices, and for protective coatings [44].

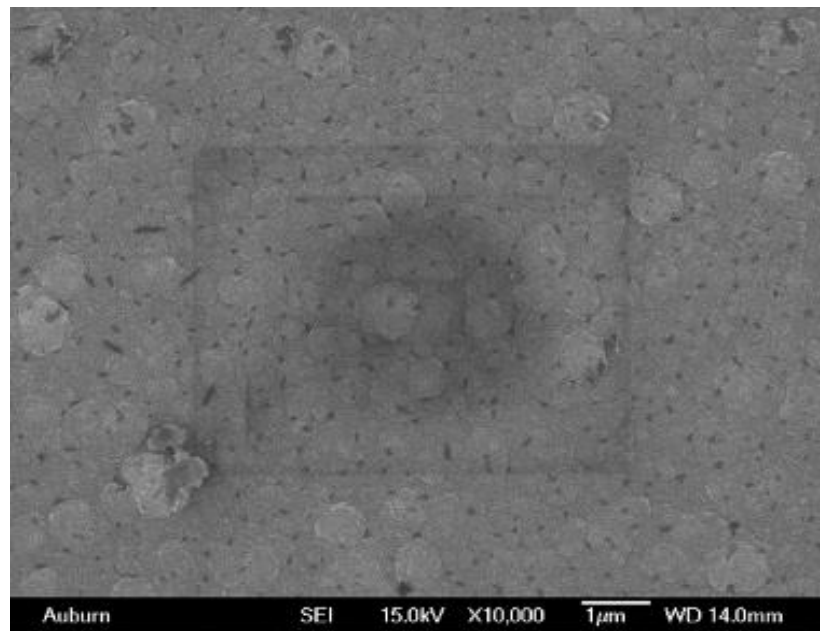


Figure 4.21 SEM images of nanocrystalline diamond surface with 10,000 resolution

The synthesis of nanocrystalline diamond films has become a mature CVD technique in the past decade. By adding noble gas, typically argon, into traditional CH₄ / H₂ gas mixtures, the nanocrystalline diamond thin films composed of 3 - 15 nm crystallites are deposited [45]. A SEM image taken from a nanocrystalline diamond sample surface is shown in Figure 4.21.

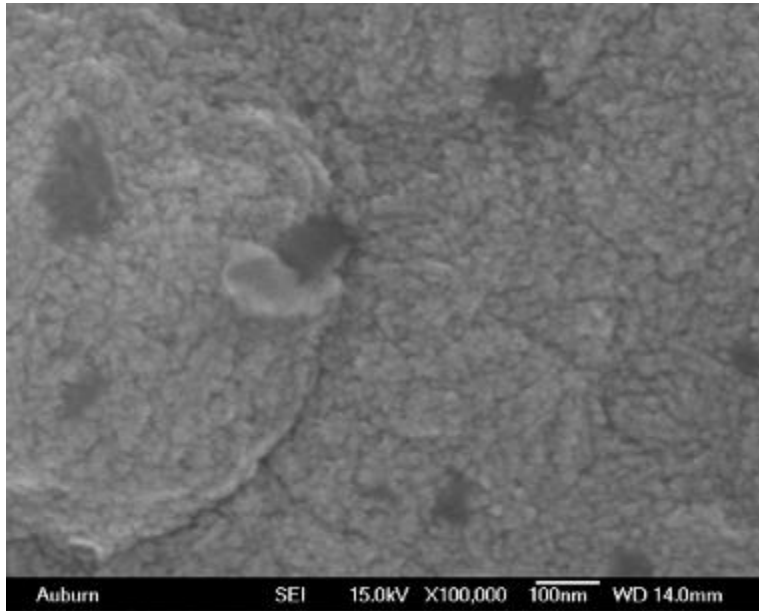


Figure 4.22 SEM images of nanocrystalline diamond surface with 100,000 resolution

There was no field emission from sample at high vacuum. Figure 4.23 and Figure 4.24 show field emission intensity of nanocrystalline diamonds at pressure of 10^{-1} Torr and 5×10^{-1} Torr, respectively. As we can see from the Figures, nanocrystalline diamond starts to emit electrons at around $2 \text{ V}/\mu\text{m}$ and the saturation emission current can be up to $10^{-4} \text{ A}/\text{cm}^2$. From Figure 4.23, it is shown that at pressure of 10^{-1} Torr, the electrons start emitting at the field intensity of about $2.1 \text{ V}/\mu\text{m}$. Additionally, the maximum emission current can only reach up to $10^{-5} \text{ A}/\text{cm}^2$. At pressure of 5×10^{-1} Torr, the field emission begins at about the same as at pressure of 10^{-1} Torr, but the maximum emission current intensity increases up to $10^{-4} \text{ A}/\text{cm}^2$.

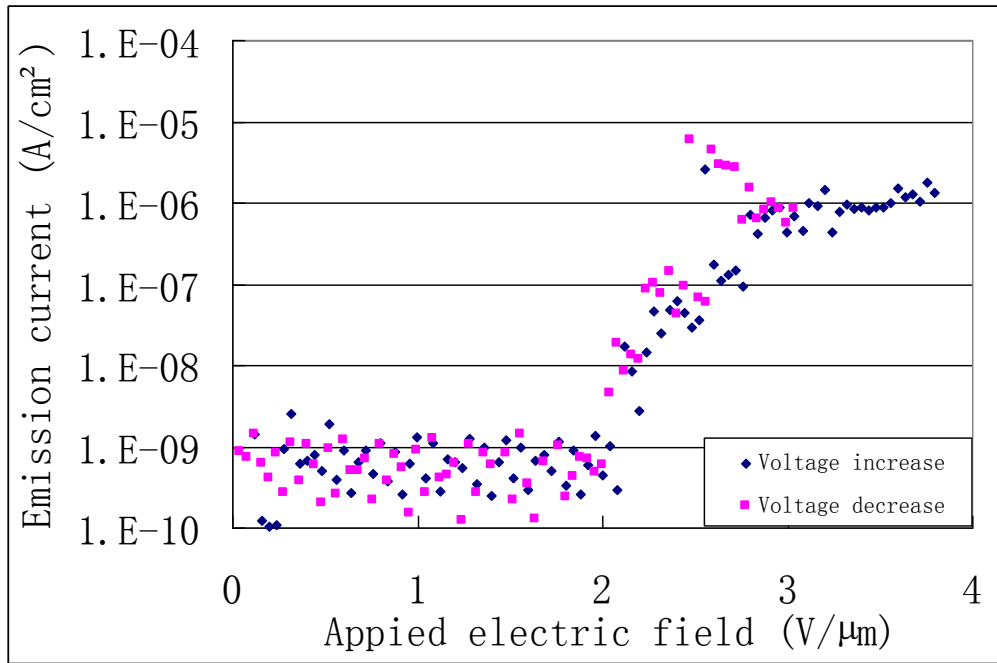


Figure 4.23 Field emission characteristic of nanocrystalline diamond at pressure of 10^{-1} Torr

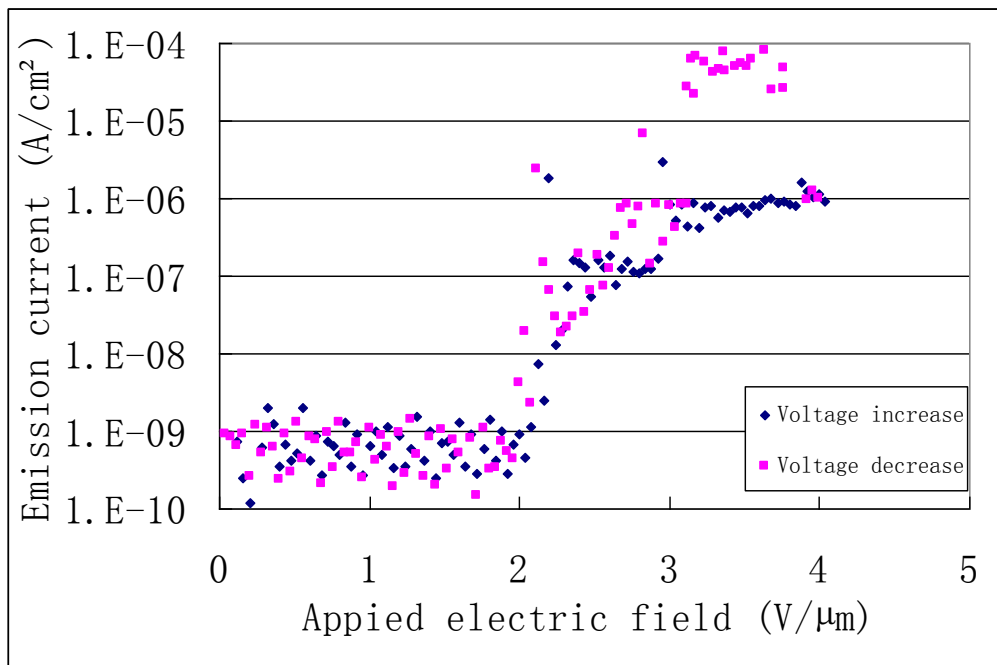


Figure 4.24 Field emission characteristic of nanocrystalline diamond at pressure of 5×10^{-1} Torr

CHAPTER 5

SUMMARY

Pseudospark switches are characterized by rapid switch time and high conducting current while operating in the glow discharge mode due to the hollow-cathode and hollow-anode geometry used in the construction. The triggering method is critical for the performance of pseudospark switch since it can greatly affects the operating characteristics such as delay, jitter, and repetition of these switches.

The seed electrons needed to initiate a breakdown can be generated by several means such as thermionic, field, or optical emission. While the thermionic emission has been used mainly in vacuum tubes and is a mature technology, field emission (or cold-cathode electron emission) has been the subject of recent studies and technology. The efficiency of these seed electron emission determines how well the plasma switch can close or open.

This work presents 6 different candidate materials and their field emission characteristics. Table 5.1 shows the comparison of the turn on electrical fields and saturation current densities of them.

In this work, it is determined that that carbon nanotubes (CNTs) are prime candidates as the source of seed electrons to trigger the switch, since they have excellent field emission characteristics under pseudospark switches operating pressure.

Table 5.1 Comparison of different materials field emission

Materials	Pressure	E_{Turn on}	Saturation current
Random MWCNT	2×10^{-6} Torr	0.8 V/ μ m	1×10^{-3} A/cm ²
	2×10^{-2} Torr	1 V/ μ m	1×10^{-3} A/cm ²
Aligned MWCNT	2×10^{-6} Torr	0.6 V/ μ m	8×10^{-4} A/cm ²
	2×10^{-2} Torr	1.1 V/ μ m	5×10^{-4} A/cm ²
Random SWCNT	2×10^{-6} Torr	0.3 V/ μ m	1×10^{-3} A/cm ²
	2×10^{-2} Torr	0.6 V/ μ m	1×10^{-3} A/cm ²
Nanorod ZnO	1×10^{-6} Torr	1.5 V/ μ m	1×10^{-3} A/cm ²
	2×10^{-2} Torr	2.2 V/ μ m	1×10^{-4} A/cm ²
Copper	4×10^{-6} Torr	5 V/ μ m	1×10^{-4} A/cm ²
	2×10^{-2} Torr	12.5 V/ μ m	1×10^{-5} A/cm ²
Nanocrystalline diamond			
	2×10^{-2} Torr	2.0 V/ μ m	1×10^{-4} A/cm ²

Since pseudospark switch operates at pressure range from 1 mTorr to 1 Torr, the field emission intensity at pressure of 2×10^{-2} Torr makes more sense than at 2×10^{-6} Torr. Among these samples, Random SWCNT possesses the lowest turn on electrical field which is 0.6 V/ μ m at pressure of 2×10^{-2} Torr. The Random MWCNT and The Aligned MWCNT have about the same turn on electrical field, 1V/ μ m and 1.1 V/ μ m, respectively. The turn on electrical fields of Nanocrystalline diamond and nanorod ZnO are 2.0V/ μ m and 2.2V/ μ m. The oxygen free copper has the highest turn on field of 12.5 V/ μ m.

From the saturation current line, we can see that the Random MWCNT and Random

SWCNT gain the highest current density 1×10^{-3} A/cm². Aligned MWCNT's saturation current is slightly smaller than the rest of them. The saturation currents of nanodiamond and nanorod ZnO are about the same: 1×10^{-4} A/cm². The smallest saturation current of these six materials is 1×10^{-5} A/cm², which is emitted by Oxygen-Free Coppers.

Basically, the lower $E_{\text{turn on}}$ the material has, the easier it can emit electrons and the higher the saturation current is, the more electrons are emitted from the surface of the samples. From this point of view, carbon nanotubes are ideal to be used as trigger materials, especially the Random SWCNT, which has the lowest $E_{\text{turn on}}$ and highest saturation current density. Although Random MWCNT and Aligned MWCNT are not as good as Random SWCNT, they have a low $E_{\text{turn on}}$ and still should be considered as promising materials. Compared to carbon nanotubes, the other two nano materials, nanocrystalline diamond and nanorod ZnO, have higher $E_{\text{turn on}}$ and lower saturation current density. However, both of them are still considered as good candidates for trigger materials. Oxygen free copper, being the traditional good conductor material, did not yield good turn on voltage and saturation current. Although, it is a good conductor, it is not a good field emitter material compared to the ones studied in this Thesis.

Future research will concentrate on building an appropriate pseudospark switch and measuring the plasma and trigger characteristics by using the above trigger electrode materials.

REFERENCES

- [1] H. Kirkici and D. Bruno, “*Operating characteristics of a segmented hollow cathode over a wide pressure range,*” IEEE Trans. on Plasma Science, Vol. 23, pp:229 - 234,1995
- [2] A. Gortler, J. Christiansen, R. Dotzer, K. Frank, “*Investigations of pulsed surface flashovers for the triggering of pseudospark high-power switches,*” IEEE Trans. on Plasma Science, Vol. 17, pp:762 – 765, 1989
- [3] C. Jiang, E.B. Sozer, R.J. Umstadd, H. Chen, H. Hsu, M.A. Gundersen, “*Photocathodes for Compact Optical Triggering of Back-Lighted Thyratrons,*” Proceedings of the 2008 IEEE IPMHVC, Page(s):477 – 479, 27-31 May 2008
- [4] S. Iijima, “*Helical microtubules of graphitic carbon,*” Nature, vol. 354, pp. 56-58, 1991
- [5] A.G. Rinzler, J.H. Hafner, P. Nikolaev, L. Lou, S.G. Kim, D. Tomanek, D. Colbert, and R.E. Smalley, “*Unraveling nanotubes: field emission from an atomic wire,*” Science, vol. 269, pp. 1550-1553, 1991
- [6] Hansjoachim Bluhm, *pulse power systems principles and applications, 2006*
- [7] Esin B Sozer, Kalyan Koppisetty, Hulya Kirkici, *Pulsed Hollow Cathode Discharge Characteristics*, Pulsed power conference, 16th IEEE International, 2007
- [8] R. Tkotz, M. Schlaug, J. Christiansen, K. Frank, A. Gortler, and A. Schwandner, *Triggering of Radial Multichannel Pseudospark Switches by a Pulsed Hollow Cathode Discharge*, plasma science, IEEE transaction on, 1996
- [9] Sozer Esin, *Gaseous Discharges and Their Applications as High Power Plasma Switches*, Thesis 2008
- [10] Gortler, A.; Christiansen, J.; Dotzer, R.; Frank, K.:Plasma Science, IEEE Transactions on

- [11] K. Frank, E. Boggasch, J. Christiansen, *High-Power Pseudospark and BLT Switches*, IEEE TRANSACTIONS ON PLASMA SCIENCE, VOL. 16, NO. 2, APRIL 1988
- [12] G. Kirkman and M. Gundersen, "*The Back-Lighted Thyatron*," in *Gas Discharge Closing Switches*. vol. 2, G. Schaefer, M. Kristiansen, and A. Guenther, Eds. New York: Plenum Press, 1990, pp. 531-541
- [13] Jiang, C.; Sozer, E.B.; Umstattd, R.J.; Chen, H.; Hsu, H.; Gundersen, M.A. *Photocathodes for Compact Optical Triggering of Back-Lighted Thyatrons*, IEEE International Power Modulators and High Voltage Conference, 2008
- [14] C. Liu, Q. Wu, X.Z., "Synthesis and Electron Emission Properties of Aluminum Nitride Nano-cones" The 5th International Vacuum Electron Sources Conference, 2004, 10.1109/IVESC.2004.1414221
- [15] Shim, J.Y.; Chi, E.J.; Baik, H.K.; "Field Emission Characteristics Of Amorphous Carbon And Diamond Emitters"; Vacuum Microelectronics Conference, 1996. IVMC'96., 9th International; 10.1109/IVMC.1996.601827
- [16] Huang, W.Y.; Liu; "Field Emission Characteristics of Polymethyl Methacrylate Polymer Thin Film"; Vacuum Nanoelectronics Conference, 2006 and the 2006 50th International Field Emission Symposium., IVNC/IFES 2006. Technical Digest, 19th International; 10.1109/IVMC.1996.601827
- [17] A.N. Ionov', E.O. Popov', A.A. Pashkevich', "Field Emission From Metal Covered By Film Of Polymer Insulator" Vacuum Electron Sources Conference, 2004. Proceedings. IVESC 2004. The 5th International; 10.1109/IVESC.2004.1414142

- [18] Deng Jicai; Zhang Binling, “*Field Emission from Metal-Coated Nano-Crystalline Graphitic Films*”, Vacuum Nanoelectronics Conference, 2006 and the 2006 50th International Field Emission Symposium., IVNC/IFES 2006. Technical Digest. 19th International ; 10.1109/IVNC.2006.335469
- [19] R.D. Underwood, D. Kapolnek, “*Field Emission From Selectively Regrown GaN Pyramids*” Device Research Conference, 1996. Digest. 54th Annual, 10.1109/DRC.1996.546417
- [20] S.Z.Deng, H.T.Xu, X.G.Zhen, “*Effect of Temperature on Field Emission Properties from Nanoclusters of Tungsten Oxide on Silicon Carbide*”, Vacuum Microelectronics Conference, 2003. Technical Digest of the 16th International
- [21] S. Iijima, “*Helical microtubules of graphitic carbon,*” *Nature*, vol. 354, pp. 56-58, 1991
- [22] S. J. Tans, A. R. M. Verschueren, and C. Dekker, *Nature (London)* 393, 49, 1998.
- [23] A. Javey, H. Kim, M. Brink, Q. Wang, A. Ural, J. Guo, P. McIntyre, P. McEuen, M. Lundstrom, H. J. Dai, *Nat. Mater.* **1**, 241, 2002
- [24] A. Javey, J. Guo, Q. Wang, M. Lundstrom, H. J. Dai, *Nature* 424, 654, 2003
- [25] S. Rosenblatt, Y. Yaish, J. Park, J. Gore, V. Sazonova, and P. L. McEuen, *Nano Lett.* **2**, 869, 2002.
- [26] C. Lu, Q. Fu, S. Huang, and J. Liu, *Nano Lett.* **4**, 623, 2004.
- [27] S. Huang, M. Woodson, R. Smalley, G. P. Siddons, D. Merchin, J. H. Back, J. K. Jeong, and M. Shim, *Nano Lett.* **4**, 927, 2004.
- [28] S. J. Tan, M. H. Devoret, H. J. Dai, A. Thess, R. E. Smalley, L. J. Geerligs, and C. Dekker, *Nature (London)* 386, 474, 1997.
- [29] M. Bockrath, D. H. Cobden, and P. L. McEuen, *Science* 290, 1552, 2000.
- [30] H. J. Dai, J. H. Hafner, A. G. Rinzler, D. T. Colbert, and R. E. Smalley, *Nature (London)*

- 384, 147, 1996.
- [31] W. A. de Heer, A. Chatelain, and D. Ugarte, *Science* 270, 1179, 1995.
- [32] A. G. Rinzler, J. H. Hafner, P. Nikolaev, L. Lou, S. G. Kim, D. Tomanek, P. Nordlander, D. T. Colbert, and R. E. Smalley, *Science* 269, 1550, 1995.
- [33] P. G. Collins, K. Bradley, M. Ishigami, and A. Zettle, *Science* 287, 1801, 2000.
- [34] J. Kong, N. R. Franklin, C. Zhou, M. G. Chapline, S. Peng, K. Cho, and H. Dai, *Science* 287, 622, 2000.12
- [35] R. J. Chen, S. Bangsaruntip, K. A. Drouvalakis, N. W. S. Kam, M. Shim, Y. M. Li, W. Kim, P. J. Utz, and H. J. Dai, *P. Natl. Acad. Sci. USA* 100, 4984, 2003.
- [36] A. Star, J. C. P. Gabriel, K. Bradley, and G. Gruner, *Nano Lett.* 3, 459, 2003.
- [37]. <http://www.godunov.com/bucky/buckyball-3.gif>
- [38] An-jen Cheng, *Cold Cathodes for Applications in Poor Vacuum and Low Pressure Gas Environments: Carbon Nanotubes Versus Zinc Oxide Nanoneedles*, Thesis, 2006
- [39] Dresselhaus, M. S., Dresselhaus, G., and Eklund, P. C., 1996
- [40] Ajayan, P. M. and Ebbesen, T. W., *Rep.Prog.Phys.*, 60, 1025-1065, 2003
- [41] Niyogi, S., Hamon, M. A., Hu, H., Zhao, B., Bhowmik, P., Sen, R., Itkis, M. E., and Haddon, R. C. *Accounts of Chemical Research*, 35, (12), 2002
- [42]. Avouris, P., *Chemical Physics*, 281, (2-3), 429-445, 2002
- [43] Tans, Sander J., Devoret, Michel H., Dal, Hongjie, Thess, Andreas, Smalley, Richard E., Geerligs, L. J. and Dekker, Cees, *Nature (London)*, 386, (6624), 1997
- [44] M. Daenen, R.D. de Fouw, B. Hamers, *The Wondrous World of Carbon Nanotubes*, February 2003
- [45] Yu-Chun Chen, *Diamond Chemical Vapor Deposition and Practical Application*, dissertation, 2009

- [46] Jung, S. H., Kim, M. R., Jeong, S. H., Kim, S. U., Lee, O. J., Lee, K. H., Suh, J. H., and Park, C. K., *Applied Physics A-Materials Science & Processing*, 76, (2), 85-286, 2003
- [47] S. Seraphin, D. Zhou, J. Jiao, J. C. Withers, R. Loufty, *Carbon*, 31, 685, 1993
- [48] T. Guo et al. *J. Phys. Chem.* 99, 10694, 1995
- [49] Bhushan editor, "*Handbook of Nanotechnology*", Springer
- [50] M. Meyyappan, editor, "*Carbon nanotubes science and applications*", CRC Press, 2004